Temporal patterning of apical progenitors and their daughter neurons in the developing neocortex

Telley, Ludovic; Agirman, Gulistan; Prados, Julien; Amberg, N; Fievre, Sabine; Oberst, Polina; Bartolini, Giorgia; Vitali, Ilaria; Cadilhac, Christelle; Hippenmeyer, S; Nguyen, L; Dayer, Alexandre; Jabaudon, Denis

How to cite

TELLEY, Ludovic et al. Temporal patterning of apical progenitors and their daughter neurons in the developing neocortex. In: Science, 2019, vol. 364, n° 6440, p. eaav2522. doi: 10.1126/science.aav2522

This publication URL: https://archive-ouverte.unige.ch/unige:126160

Publication DOI: 10.1126/science.aav2522

Temporal patterning of apical progenitors and their daughter neurons in the developing neocortex

L. Telley[1,3*†], G. Agirman[1,4†], J. Prados[1], N. Amberg[6], S. Fièvre[1], P. Oberst[1], G. Bartolini[1], I. Vitali[1], C. Cadilhac[1], S. Hippenmeyer[6], L. Nguyen[4], A. Dayer[1,5], D. Jabaudon[1,2*]

[1] Department of Basic Neurosciences, University of Geneva, Geneva, Switzerland.

[2] Clinic of Neurology, Geneva University Hospital, Geneva, Switzerland.

[3] Current address: Department of Basic Neuroscience, University of Lausanne, Switzerland.

[4] GIGA-Stem Cells, University of Liège, C.H.U. Sart Tilman, Liège, Belgium.

[5] Department of Psychiatry, Geneva University Hospital, Geneva, Switzerland.

[6] Institute of Science and Technology Austria, Klosterneuburg, Austria.

[†] equally contributed to this work.

[*] Correspondence to: ludovic.telley@unil.ch; denis.jabaudon@unige.ch

Abstract

During corticogenesis, distinct subtypes of neurons are sequentially born from ventricular zone progenitors. How these cells are molecularly temporally patterned is unknown. Here, we use high temporal resolution single-cell RNA sequencing to lineage-trace the molecular identities of successive generations of apical progenitors (APs) and their daughter neurons in mouse embryos. We identify a core set of evolutionarily-conserved, temporally-patterned genes, which drive APs from internally-driven to more exteroceptive states, and reveal that the polycomb repressor complex PRC2 epigenetically regulates AP temporal progression. Embryonic age-dependent AP molecular states are transmitted to their progeny as successive ground states, onto which essentially conserved early post-mitotic differentiation programs are applied, and complemented by later occurring environment-dependent signals. Thus, epigenetically-regulated temporal molecular birthmarks present in progenitors act in their post-mitotic progeny to seed adult neuronal diversity.

One Sentence Summary: During corticogenesis, temporally dynamic molecular birthmarks present in progenitors act as seeds for neuronal diversity in their post-mitotic progeny.

Main Text

Adult neuronal diversity emerges from the interaction between progenitor-derived genetic information and environment-derived signals, but how these processes unfold and interact in the developing brain is still unclear. In the neocortex, whose neurons are required for high-order cognitive and sensorimotor information processing in mammals, the temporal molecular patterning of progenitors is thought to be a driving force for their progression in neurogenic competence (*1-3*). Such temporal patterning is an evolutionarily-conserved strategy to generate neuronal diversity, but in contrast to Drosophila, in which key molecules of temporal specification have been identified (*4*), how this occurs in mammals remains poorly understood. Although the single-cell diversity of the neocortex is increasingly well characterized (*5-11*), how temporally progressing pre- and post-mitotic programs in APs and neurons interact to give rise to the neuronal diversity of the adult neocortex remains unknown. One reason for this has been the lack of a technique allowing the precise dissection of temporal transcriptional states in specific cells types. Here, we overcome this limitation by using FlashTag (FT), a high temporal resolution method to pulse-label APs and their daughter neurons (*12*, *13*) and trace the transcriptional trajectories of successive generations of progenitors and isochronic cohorts of their daughter neurons from embryonic day (E) 12 to E15, as layer (L) 6, L5, L4 and L2/3 neurons are successively generated (*3*).

Identifying dynamic transcriptional states in APs and neurons

Following microdissection of the putative somatosensory cortex, we collected FT^+ cells by FACS after either 1 h, as APs are still dividing, 24 h, as daughter cells are transiting through the subventricular zone, or 96 h, once daughter neurons have entered the cortical plate (Fig. 1A and fig. S1, A-D). We performed single-cell RNA sequencing at each of these 3 differentiation stages at 4 embryonic ages (E12, E13, E14, and E15), which yielded a total of 2,756 quality-controlled cells across 12 conditions for analysis (fig. S1, C and D, and Methods).

Analysis of cellular transcriptional identities using t-SNE dimensionality reduction first revealed that cells were organized based on collection time, *i.e.* differentiation status: 1 h-, 1-day- and 4-day-old cells formed three main groups of cells which corresponded essentially to (1) APs, (2) basal progenitors (BPs) and 1-day-old neurons (N1d), and (3) 4-day-old neurons (N4d), as indicated by the combined expression of type-specific markers (Fig. 1B) (*12*). At each of these differentiation stages, cells born at successive embryonic ages tended to cluster together, forming chronotopic maps, which were particularly apparent for APs and 1-day-old daughter cells, but less striking, although still discernable, in 4-day-old neurons. This suggests that birthdate-related transcriptional features are strong determinants of AP and of initial neuron identity, but also that non-birthdate-related programs are implemented during differentiation.

Together, these data reveal two axes of transcriptional organization: a birthdate axis, corresponding to the temporal progression in AP transcriptional states at sequential embryonic ages, and which also emerged from unbiased analysis of single-cell trajectories (Monocle) (fig. S1E) (*14*), and a differentiation axis, corresponding to the birth and maturation of their daughter neurons. These two cardinal processes are thus the major source of transcriptional diversity in the developing neocortex.

We used a graph-based cluster analysis to investigate the diversity of differentiation stage- and birthdate-specific cells (Fig. 1C) and differential expression analysis to identify type-enriched transcripts, whose temporal patterns of expression were confirmed by *in situ* hybridization (Fig. 1D and E; figs. S2 and S3; data table S1 and see also http://genebrowser.unige.ch/telagirdon/). Cluster analysis identified four embryonic age-defined AP transcriptional states, as well as two embryonic age-defined basal progenitor populations, as recently reported (*15*) (Fig. 1C). Two classes of 1-day-old neurons (N1d) could be distinguished, early-born cells (*i.e.* E12-E13-born) and later-born cells (*i.e.* E14-E15-born). These two classes of neurons displayed early onset expression of deep- and superficial-layer genes, which foreshadowed their upcoming lamina-related identity. Early on, however, classical deep-layer markers were also expressed by late-born neurons (fig. S4A), as previously reported (*16*, *17*). By four days of age, however, neurons with mutually-exclusive expression of classical lamina-specific markers such as *Bcl11b* (a L5 / deep layer marker), *Rorb* (L4) and *Pou3f2* (L2/3) emerged (Fig. 1C, right and fig. S4, A and B). Thus, late-born neurons initially transiently display some molecular features of earlier-born neurons, which they repress as they undergo fate refinement.

Of note, in addition to these VZ-born cell populations, two types of non-VZ-born cells were detected. First, GABAergic interneurons, the bulk of which emerged 4 days after FT labeling, consistent with migration into the dorsal pallium after FT labeling of their progenitors in the ventral pallium (*18*, *19*) (Fig. 1C and fig. S4C). Interestingly, a small fraction of these interneurons (16%) was detected 1h after FT labelling, especially at late embryonic stages, supporting reports of inhibitory interneurons migrating radially to contact the ventricle in the dorsal pallium late in corticogenesis (*20*, *21*). Second, astrocytes, exclusively detected 4 days after E15 FT labeling (*i.e.* at P0), which likely correspond to ventral pallium-born astrocytes migrating into the cortex (*22*, *23*) (Fig. 1C and fig. S4D). These two cell types were not further investigated in this study. Together, these results indicate that APs transit through temporally dynamic transcriptional states during corticogenesis as daughter neurons progressively acquire type-specific transcriptional features.

APs progress from "introverted" to "extraverted" transcriptional states

We used two axes of investigation to address the transcriptional dynamics of differentiating neurons and of APs: we studied on the one hand the transcriptional differentiation of neurons born on each embryonic day between E12 and E15 (Fig. 2A-C), and on the other hand, the progression in AP transcriptional states during this time period, as shown in Fig. 2D-F.

We first examined the transcriptional programs expressed by differentiating neurons born on each embryonic age (Fig. 2A-C). For this purpose, we used an unsupervised approach in which single cells were unbiasedly ordered on a linear path based on their transcriptional profile (*24*). This pseudotime (*i.e.* pseudo-differentiation) alignment approach outlined successive transcriptional waves driving differentiation (*12*) (Fig. 2A, fig. S5, and data table S2). Remarkably, the sequential unfolding of gene expression was essentially conserved across embryonic ages, as revealed by closely matching gene expression dynamics (Fig. 2B and fig. S5A-E). Constant gene expression did not simply reflect the constant activity of a small number of "pan-neuronal" genes (*e.g. Neurod2*) but instead reflected tightly overlapping differentiation programs since over half of the expressed genes had highly correlated expression dynamics (R>.7, fig. S5C). Accordingly, gene ontologies were conserved across embryonic ages (Fig. 2C, fig. S5F, and data table S3). Thus, neuronal differentiation programs appear largely conserved across corticogenesis.

We next addressed the temporal progression in AP transcriptional states, using the approach described above. This pseudotime alignment approach appropriately ordered E12-, E13, E14-, and E15-dividing APs, effectively constituting a pseudo-birthdate axis (Fig. 2D). This allowed us to determine individual gene expression dynamics in APs across corticogenesis, which were reflected in *in situ* hybridization temporal series (Fig. 2E, fig. S6A-C, and data table S4). Clustering of transcripts based on their expression dynamics showed how transcriptional programs unfold in APs (Fig. 2, E and F, data tables S4 and S5). Initially (E12, E13), typically cell-intrinsic programs were at play: transcripts coding for nuclear proteins (*e.g. Rpa1*, involved in DNA replication or the *Top2A* DNA topoisomerase) and cell-cycle regulators (*e.g. Ccne1*, *E2f1*, *E2f8*) were increased, consistent with active cell cycle regulation processes. Similarly, transcripts involved in the regulation of gene expression and chromatin structure were prominent (*e.g. Hmga2,* which promotes self-renewal of neural progenitors (*25*) and *Trim27*, which interacts with the polycomb complex to repress gene expression (*26*)). Finally, cell death modulators (*e.g. Siva1*, *Scrib*) were also actively transcribed, suggesting some level of control over progenitor pool size (*27*).

Later on (E14, E15), exteroceptive, environment-sensing-related programs predominated (Fig. 2F). This included ion transport-related processes, in line with a bioelectrically-controlled progression of AP competence (*28*), and consistent with the increased frequency of calcium waves in APs later in corticogenesis (*29*). Similarly, cell-cell and cell-matrix interaction related processes (*e.g. Bcan*) increased, as did lipid metabolism-related genes (*e.g. Fabp7*, *Acadvl*) , which has been linked with progenitor fate in adult neuronal stem cells (*30*). In line with the induction of exteroception-related programs, late APs also expressed genes typically associated with neuron-related processes such as synaptogenesis and neurotransmission, suggesting that corresponding exteroceptive programs are progressively implemented in successive generations of APs and in their post-mitotic neuronal progeny. Finally, glia-related processes emerged, foreshadowing the upcoming generation of this cell type later in corticogenesis. Together, these data suggest that as corticogenesis unfolds, APs shift from mostly internally-driven programs to environment sensing ones (Fig. 2G).

We used two examples to illustrate the functional correlates of this progression in transcriptional states. First, we investigated the net effect of the dynamics of cell-cycle control-related transcripts (which predominate at early stages) by measuring cell cycle duration

specifically in APs ($SOX2^+$ cells) (Fig. 2H). This revealed a ~50% increase in cell cycle length between E12 and E15 (from 8h to 12h), confirming and extending previous results (*31*, *32*). Lengthening of the cell cycle essentially reflects a lengthening of G1, a critical phase for environment sensing and fate decision (refs *31*, *33*, *34*, and fig. S6D), such that this progression in cycling dynamics is congruent with the overall progression in AP behavior during corticogenesis.

A second example was provided by the glutamate transporter transcript *Slc1a3* (*Glast*), whose expression increases in APs as glutamatergic neurotransmission develops in the cortical plate (Fig. 2I). To directly investigate whether increased *Glast* transcriptional activity was accompanied by an increase in glutamate uptake by APs, we used DL-threo-β-Benzyloxyaspartic acid (TBOA) to block this electrogenic transporter at distinct embryonic stages (*35*), and measured evoked currents using whole-cell patch clamping of APs, identified as juxtaventricular cells (*13*). Pharmacological blockade of this transporter increased glutamate levels at late, but not early embryonic stages, consistent with a dynamic bioelectrical control over AP properties during corticogenesis (Fig. 2I) (*28*). Thus, the transcriptional progression from mostly internally-driven processes to environment-sensing ones is accompanied by a corresponding functional progression in AP biological properties.

APs and daughter neurons share molecular temporal identities

The differentiation programs of daughter neurons are largely conserved across embryonic ages, despite the distinct identities these daughter neurons acquire later. How then does neuronal diversity emerge? As reported above, the chronotopic arrangement of APs is also present in their 1-day old progeny (Fig. 1B). This suggests that embryonic age-dependent AP transcriptional programs are transmitted to their progeny to generate successive initial neuronal identities. To investigate this possibility, we next determined how dynamic transcriptional networks emerge in single cells during corticogenesis. We used a machine learning strategy to classify cells based on (1) their birthdate and (2) their differentiation status, which identified core sets of genes (n = 100 per model) sufficient to classify all cells according to these two cardinal features (Fig. 3A, fig. S7A-C, and data table S6), many of which have been previously involved in regulating progenitor and neuronal fate (tables S1 and S2). Birthdate-associated core genes were sequentially expressed by APs and their 1- and 4-day old progeny, revealing a shared temporal patterning of mother and daughter cells (Fig. 3B, top and fig. S7D). On the other hand, the dynamics of the differentiation

geneset were conserved across embryonic ages, consistent with a consensus post-mitotic differentiation program, as identified earlier (Fig. 3B, bottom). This process is an evolutionarily-conserved one, since in human embryos, the transcriptional dynamics of the orthologs of this geneset and the corresponding temporal patterning of daughter neurons and their mother cells was conserved in a large dataset of cortical cells (*7*) (Fig. 3C). Thus, the temporal patterning process identified here constitutes a conserved strategy to generate neuronal diversity during corticogenesis. Consistent with the increase in neuron-related ontologies in APs noted above, expression of the neuronal differentiation geneset progressively increased in APs as corticogenesis unfolded (fig. S7, E and F); the latter cells thus become progressively "neuronized" as they give rise to successive generations of post-mitotic daughter cells. Taken together, these data reveal an evolutionarily conserved specification process in which neuron-type identities emerge from temporally-defined transcriptional ground states present in their mother cell, onto which essentially conserved post-mitotic differentiation programs are applied (Fig. 3D).

Role of the environment in refining neuronal identity

The corresponding temporal birthmarks of newborn neurons and their mother AP could in principle reflect either a lineage-related process (*i.e.* the vertical transmission of a transcriptional state from mother to daughter cell) or an environmental process in which both cells synchronously respond to progressing temporal environmental cues. To distinguish between these two possibilities, we reasoned that if environment factors were driving daughter neuron temporal identity, then the temporal patterning of postmitotic neurons would be less distinct *in vitro* than *in vivo*. We thus isolated FT^+ APs at E12 and E15 *in vitro* and examined the fate of their daughter neurons. Using combined expression of CTIP2 (BCL11B, an early-born neuron marker) and BRN2 (POU3F2, a late-born neuronal marker) to molecularly distinguish neurons born from E12 or E15 APs (fig. S4B and fig. S8A), we found that as was the case *in vivo*, the temporal identities of E12 and E15 APs progenies remained sharply defined *in vitro* (fig. S8). Together with the conserved ability of cortical progenitors to generate successive populations of neurons *in vitro* (*1*, *36*), these findings support a largely vertical transmission of temporal birthmarks from mother to daughter cells.

Although the environment does not appear to drive the initial identity of newborn neurons, temporal patterning fades with differentiation (see the partial loss in the chronotopic mapping in Fig. 1B), suggesting that non-birthdate-related processes come into play as neurons mature. To examine how temporal birthmarks evolve with neuronal differentiation, we applied the pseudotime alignment approach used above to N1d and N4d and compared it with the results obtained with APs. This revealed an overall fading of temporal patterning with differentiation, which was particularly striking for E14-born neurons, which will differentiate into L4 neurons and whose final identity strongly depends on environmental input (*37*) (Fig. 4A). Consistent with the progressive implementation of environment-driven programs, functionally relevant input-dependent transcripts such as *Nrn1* and *Rorb* (*12*, *37-39*) progressively increased in E14-born neurons as they matured (Fig. 4B). Together with the temporal progression in AP exteroceptive programs, these findings suggest that the relative importance of genetic and environmental factors shifts towards the latter as neurons differentiate and corticogenesis proceeds (Fig. 4C).

Mapping dynamic transcriptional landscapes during corticogenesis

We combined the two aforementioned models to identify birthdate- and differentiation stage-related patterns of gene expression. Based on the combined expression of the core genes of the two models, each cell was assigned a birthdate score and differentiation score. Cells were then embedded within a two-dimensional matrix, allowing the display of gene expression profiles as chrono-typic transcriptional maps (Fig. 5A) (*7*). This approach revealed a variety of dynamically-regulated transcriptional patterns, including within single families of genes (Fig. 5B, fig. S9, and http://genebrowser.unige.ch/telagirdon/). To identify archetypical features of gene expression, we performed a t-SNE-based cluster analysis of all transcriptional maps, revealing canonical clusters of genes with similar expression dynamics (Fig. 5C and data table S7). Genes within each of these canonical clusters shared common functions, and the distinct clusters were functionally specialized (Fig. 5D, fig. S10, and data table S8). This suggests that these transcriptional clusters represent functional units orchestrating the progression of temporal patterning during corticogenesis.

To illustrate the functional relevance of these processes in the temporal patterning of AP and neuronal identity, we examined the role of chromatin organization activity, which predominates in early APs (Fig. 2F and Fig. 5D), as a proof-of-principle process. Expression of the Polycomb Repressive Complex 2 (PRC2), which regulates histone methylation and hence

chromatin accessibility (*40*), provided a point of entry: the main core subunits of the complex were co-expressed in APs early in corticogenesis, and the H3K27me3 signature mark of PRC2 had corresponding dynamics, demonstrating temporally-gated functional activity (Fig. 6A). To directly address the role of this complex in the temporal progression of AP identity, we generated a cortex-specific knockout mouse for Eed, a regulatory subunit of PRC2 (Eed cKO mice). Loss of Eed eliminated PRC2's signature methylation mark in APs, consistent with a loss-of-function phenotype (Fig. 6B). As previously reported in the absence of another subunit of PRC2 (*41*), the thickness of the neocortex was strongly decreased in Eed cKO mice, consistent with a rapid temporal progression of APs resulting in a shortened neurogenic period. Supporting this possibility, decreases in VZ thickness and increases in cell cycle exit unfolded precociously in Eed cKO cortex compared to WT mice (Fig. 6, C and D). To directly investigate whether the neurogenic competence of $Eed^{-/-}$ APs was accelerated, we fate-mapped E14-born neurons using FT pulse-labeling. In contrast to WT cortex, in which essentially only L4 neurons are generated at this time, neurons with laminar and molecular features of normally later-born, L2/3 neurons were being generated in the Eed mutant (Fig. 6E). Together, these results reveal that PRC2 exerts a fine-grained control over the temporal unfolding of successive states in APs and their daughter neurons (Fig. 6F).

Discussion

Together, our findings identify a combinatorial process in which type-specific neuronal identity emerges from the apposition of generic differentiation programs onto embryonic age-dependent, AP-derived transcriptional states. In this scenario, neuronal differentiation essentially corresponds to the implementation of programs coding for generic neuronal features (*e.g.* neurites, neurotransmission) onto temporally-defined initial transcriptional states. This process is reminiscent of how neuron diversity is generated in evolutionary older brain regions such as the subpallium or spinal cord (*7*, *24*, *42*, *43*). In the subpallium, recent data in fact directly support largely conserved differentiation paths for distinct subtypes of inhibitory interneurons (*7*, *24*, *43*, *44*), with the difference that in these regions, distinctions in initial neuronal states reflect a predominantly spatial rather than temporal distribution of molecularly distinct progenitors. These two modes of generating neuron diversity (*i.e.* temporal or spatial patterning) are in fact related,

since the temporally-coordinated expression of genes across adjacent cells is required to delineate molecularly-defined areas. In evolutionary terms, temporal patterning may have been selected as the primary mode of neuron production within neocortical areas because it allows the generation of a large spectrum of cell types at low spatial cost.

In the course of corticogenesis, APs progressively become more exteroceptive. This suggests that extrinsic factors modulate neurogenesis late in development. Consistent with an increased receptivity of APs to their environment, their transcriptional identity shifts towards that of their neuronal progeny. This progressive acquisition of neuronal transcriptional features could reflect a decreased efficiency of the cyclic removal/insertion of epigenetic marks upon repetitive cell divisions, or the permeation of daughter neuron RNA / proteins into the mother cell.

Transmission of temporal birthmarks from mother to daughter cell may occur via conserved local- or large-scale 3D chromatin features, as suggested by the critical role of epigenetic regulation in temporal patterning identified here. In addition, the passive transmission of cytoplasmic RNA and post-transcriptional events may also be involved (*17*, *45-48*). This temporal birthmark fades with differentiation as environmental factors come into play. This process is particularly striking in developing L4 neurons, which are the main gateway for sensory input to the cortex, and whose final identity is sculpted by thalamocortical inputs (*37*). These environment-dependent processes may occur in an area-specific manner, and account for the recently-reported molecular diversity in corresponding adult neuronal types across cortical areas (*10*). It will thus be interesting in future studies to understand how these environmental factors complement and eventually override earlier transcriptional processes, culminating in the generation of the full complement of cells required for functional cortical circuits.

References and Notes:

1. N. Gaspard *et al.*, An intrinsic mechanism of corticogenesis from embryonic stem cells. *Nature*. **455**, 351–357 (2008).

2. M. Okamoto *et al.*, Cell-cycle-independent transitions in temporal identity of mammalian neural progenitor cells. *Nature Communications*. **7**, 1–16 (2016).

3. D. Jabaudon, Fate and freedom in developing neocortical circuits. *Nature Communications*. **8**, 16042 (2017).

4. M. Kohwi, C. Q. Doe, Temporal fate specification and neural progenitor competence during development. *Nature Reviews Neuroscience*. **14**, 823–838 (2013).

5. A. Zeisel *et al.*, Brain structure. Cell types in the mouse cortex and hippocampus revealed by single-cell RNA-seq. *Science*. **347**, 1138–1142 (2015).

6. B. Tasic *et al.*, Adult mouse cortical cell taxonomy revealed by single cell transcriptomics. *Nature Neuroscience*. **19**, 335–346 (2016).

7. T. J. Nowakowski *et al.*, Spatiotemporal gene expression trajectories reveal developmental hierarchies of the human cortex. *Science*. **358**, 1318–1323 (2017).

8. A. Saunders *et al.*, Molecular diversity and specializations among the cells of the adult mouse brain. *Cell*. **174**, 1015–1030.e16 (2018).

9. A. Zeisel *et al.*, Molecular architecture of the mouse nervous system. *Cell*. **174**, 999–1014.e22 (2018).

10. B. Tasic *et al.*, Shared and distinct transcriptomic cell types across neocortical areas. *Nature*. **563**, 72–78 (2018).

11. J. Kageyama, D. Wollny, B. Treutlein, J. G. Camp, ShinyCortex: Exploring single-cell transcriptome data from the developing human cortex. *Frontiers in Neuroscience*. **12**, 315 (2018).

12. L. Telley *et al.*, Sequential transcriptional waves direct the differentiation of newborn neurons in the mouse neocortex. *Science*. **351**, 1443–1446 (2016).

13. S. Govindan, P. Oberst, D. Jabaudon, In vivo pulse labeling of isochronic cohorts of cells in the central nervous system using FlashTag. *Nature Protocols*. **13**, 2297–2311 (2018).

14. C. Trapnell *et al.*, The dynamics and regulators of cell fate decisions are revealed by pseudotemporal ordering of single cells. *Nature Biotechnology*. **32**, 381–386 (2014).

15. S. A. Yuzwa *et al.*, Developmental emergence of adult neural stem cells as revealed by single-cell transcriptional profiling. *Cell Reports*. **21**, 3970–3986 (2017).

16. E. Azim, S. J. Shnider, G. Y. Cederquist, U. S. Sohur, J. D. Macklis, Lmo4 and Clim1 progressively delineate cortical projection neuron subtypes during development. *Cerebral Cortex*. **19**, i62–9 (2009).

17. S. K. Zahr *et al.*, A translational repression complex in developing mammalian neural stem cells that regulates neuronal specification. *Neuron*. **97**, 520–537.e6 (2018).

18. O. Marin, Cellular and molecular mechanisms controlling the migration of neocortical interneurons. *Eur J Neurosci*. **38**, 2019–2029 (2013).

19. B. Wamsley, G. Fishell, Genetic and activity-dependent mechanisms underlying interneuron diversity. *Nature Reviews Neuroscience*. **18**, 299–309 (2017).

20. B. Nadarajah, J. G. Parnavelas, Modes of neuronal migration in the developing cerebral cortex. *Nature Reviews Neuroscience*. **3**, 423–432 (2002).

21. Y. Yokota *et al.*, Radial glial dependent and independent dynamics of interneuronal migration in the developing cerebral cortex. *PLoS ONE*. **2**, e794 (2007).

22. J. D. Cahoy *et al.*, A transcriptome database for astrocytes, neurons, and oligodendrocytes: a new resource for understanding brain development and function. *J Neurosci*. **28**, 264–278 (2008).

23. S. Minocha *et al.*, Nkx2.1 regulates the generation of telencephalic astrocytes during embryonic development. *Sci Rep*. **7**, 43093 (2017).

24. C. Mayer *et al.*, Developmental diversification of cortical inhibitory interneurons. *Nature*. **555**, 457–462 (2018).

25. J. Nishino, I. Kim, K. Chada, S. J. Morrison, Hmga2 promotes neural stem cell self-renewal in young but not old mice by reducing p16Ink4a and p19Arf Expression. *Cell*. **135**, 227–239 (2008).

26. Y. Shimono, H. Murakami, Y. Hasegawa, M. Takahashi, RET finger protein is a transcriptional repressor and interacts with enhancer of polycomb that has dual transcriptional functions. *J Biol Chem*. **275**, 39411–39419 (2000).

27. C. L. Cunningham, V. Martinez-Cerdeño, S. C. Noctor, Microglia regulate the number of neural precursor cells in the developing cerebral cortex. *J Neurosci*. **33**, 4216–4233 (2013).

28. I. Vitali *et al.*, Progenitor Hyperpolarization Regulates the Sequential Generation of Neuronal Subtypes in the Developing Neocortex. *Cell*. **174**, 1264–1276.e15 (2018).

29. T. A. Weissman, P. A. Riquelme, L. Ivic, A. C. Flint, A. R. Kriegstein, Calcium waves propagate through radial glial cells and modulate proliferation in the developing neocortex. *Neuron*. **43**, 647–661 (2004).

30. M. Knobloch *et al.*, Metabolic control of adult neural stem cell activity by Fasn-dependent lipogenesis. *Nature*. **493**, 226–230 (2013).

31. T. Takahashi, R. S. Nowakowski, V. S. Caviness, The cell cycle of the pseudostratified ventricular epithelium of the embryonic murine cerebral wall. *J Neurosci*. **15**, 6046–6057 (1995).

32. B. Martynoga, H. Morrison, D. J. Price, J. O. Mason, Foxg1 is required for specification of ventral telencephalon and region-specific regulation of dorsal telencephalic precursor proliferation and apoptosis. *Dev Biol*. **283**, 113–127 (2005).

33. Y. Sela, N. Molotski, S. Golan, J. Itskovitz-Eldor, Y. Soen, Human embryonic stem cells exhibit increased propensity to differentiate during the G1 phase prior to phosphorylation of retinoblastoma protein. *Stem Cells*. **30**, 1097–1108 (2012).

34. A. Soufi, S. Dalton, Cycling through developmental decisions: how cell cycle dynamics control pluripotency, differentiation and reprogramming. *Development*. **143**, 4301–4311 (2016).

35. D. Jabaudon *et al.*, Inhibition of uptake unmasks rapid extracellular turnover of glutamate of nonvesicular origin. *Proc Natl Acad Sci USA*. **96**, 8733–8738 (1999).

36. M. Eiraku *et al.*, Self-organized formation of polarized cortical tissues from ESCs and its active manipulation by extrinsic signals. *Cell Stem Cell*. **3**, 519–532 (2008).

37. G. Pouchelon *et al.*, Modality-specific thalamocortical inputs instruct the identity of postsynaptic L4 neurons. *Nature*. **511**, 471–474 (2014).

38. D. Jabaudon, S. J Shnider, D. J Tischfield, M. J Galazo, J. D. Macklis, RORB induces barrel-like neuronal clusters in the developing neocortex. *Cerebral Cortex.* **22**, 996-1006 (2012).

39. E. Klingler *et al.*, A translaminar genetic logic for the circuit identity of intracortically projecting neurons. *Current Biology*. **29**, 332-339.e5 (2019).

40. R. Margueron, D. Reinberg, The Polycomb complex PRC2 and its mark in life. *Nature*. **469**, 343–349 (2011).

41. J. D. Pereira *et al.*, Ezh2, the histone methyltransferase of PRC2, regulates the balance between self-renewal and differentiation in the cerebral cortex. *Proc Natl Acad Sci USA*. **107**, 15957–15962 (2010).

42. J. S. Dasen, Transcriptional networks in the early development of sensory-motor circuits. *Development of Neural Circuitry*. **87**, 119–148 (2009).

43. D. Mi *et al.*, Early emergence of cortical interneuron diversity in the mouse embryo. *Science*. **360**, 81–85 (2018).

44. L. Telley, D. Jabaudon, A mixed model of neuronal diversity. *Nature*. **555**, 452–454 (2018).

45. K.-J. Yoon *et al.*, Temporal control of mammalian cortical neurogenesis by m6a methylation. *Cell*. **171**, 877–889.e17 (2017).

46. K.-J. Yoon, C. Vissers, G.-L. Ming, H. Song, Epigenetics and epitranscriptomics in temporal patterning of cortical neural progenitor competence. *J Cell Biol*. **217**, 1901–1914 (2018).

47. M. Z. Ozair *et al.*, hPSC Modeling reveals that fate selection of cortical deep projection neurons occurs in the subplate. *Cell Stem Cell*. **23**, 60–73.e6 (2018).

48. T. J. Nowakowski *et al.*, Regulation of cell-type-specific transcriptomes by microRNA networks during human brain development. *Nature Neuroscience*. **21**, 1784–1792 (2018).

49. M. Yu *et al.*, Insights into GATA-1-mediated gene activation versus repression via genome-wide chromatin occupancy analysis. *Molecular Cell*. **36**, 682–695 (2009).

50. J. A. Gorski *et al.*, Cortical excitatory neurons and glia, but not GABAergic neurons, are produced in the Emx1-expressing lineage. *J Neurosci*. **22**, 6309–6314 (2002).

51. S. Hippenmeyer, R. L. Johnson, L. Luo, Mosaic analysis with double markers reveals cell-type-specific paternal growth dominance. *Cell Reports*. **3**, 960–967 (2013).

52. D. Jabaudon, M. Scanziani, B. H. Gähwiler, U. Gerber, Acute decrease in net glutamate uptake during energy deprivation. *Proc Natl Acad Sci USA*. **97**, 5610–5615 (2000).

53. T. Smith, A. Heger, I. Sudbery, UMI-tools: modeling sequencing errors in Unique Molecular Identifiers to improve quantification accuracy. *Genome Research.* **27**, 491–499 (2017).

54. C. H. Teo, S. V. N. Vishwanthan, A. J. Smola, Q. V. Le, Bundle Methods for Regularized Risk Minimization. *Journal of Machine Learning Research*. **11**, 311–365 (2010).

55. P. Shannon *et al.*, Cytoscape: a software environment for integrated models of biomolecular interaction networks. *Genome Research.* **13**, 2498–2504 (2003).

56. S. Maere, K. Heymans, M. Kuiper, BiNGO: a Cytoscape plugin to assess overrepresentation of gene ontology categories in biological networks. *Bioinformatics*. **21**, 3448–3449 (2005).

Acknowledgments:
We thank A. Benoit and the Genomics Platform and FACS Facility of the University of Geneva for technical assistance; and H. Wu, E. Azim, O. Raineteau, D. Silver and the members of the Jabaudon laboratory for comments on the manuscript. Illustration in panel 3D: www.lagraphisterie.fr. **Funding:** Work in the Jabaudon laboratory is supported by the Swiss National Science Foundation and the Carigest Foundation. DJ and AD are supported by the Fondation privée des HUG. G.A. is a PhD student from the F.R.S-F.N.R.S and is supported by the Fonds Léon Fredericq. The LN laboratory is funded by the F.R.S.-FNRS (EOS O019118F-RG36; CDR J.0028.18; PDR T.0073.15) the Fonds Léon Fredericq, the Fondation Médicale Reine Elisabeth, and the Fondation Simone et Pierre Clerdent. A.D. is funded by the Swiss National Science Foundation and the National Center of Competence in Research (NCCR) Synapsy. Work in the Hippenmeyer laboratory is supported by IST Austria institutional funds and the European Research Council (ERC) under the European Union's Horizon 2020 Research and Innovation Program (grant agreement No 725780 LinPro). NA is supported by the FWF Hertha Firnberg Program (grant No T 1031-BBL).

Author contributions: LT and GA performed the experiments with the help of PO and IV. LT, GA and JP performed the bioinformatic analysis. SF performed the electrophysiology experiments. CC performed the smFISH experiment. GB performed the *in vitro* experiments. NA performed the Eed cKO-related experiments. GA, DJ and LT wrote the manuscript with the help of AD, LN and SH. **Competing interests:** none. **Data and materials availability:** All annotated data are available at the GEO database (accession number: GSE118953) or in the open access website (http://genebrowser.unige.ch/telagirdon/). The supplementary materials contain additional data.

Supplementary Materials:

Materials and Methods

References (*49-56*)

Figures S1-S10

Tables S1, S2

External Databases S1-S8

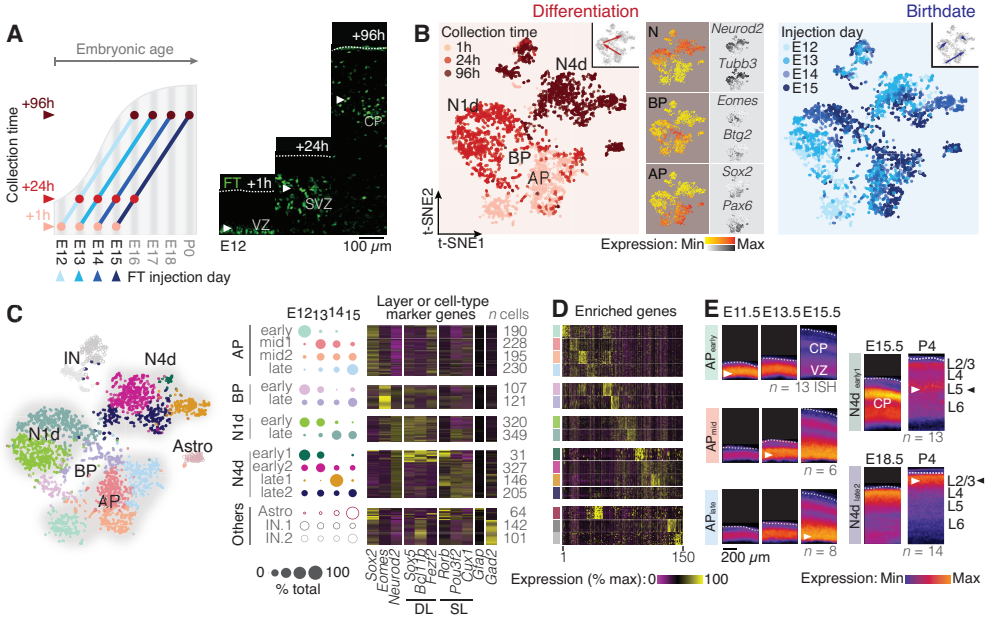

Figure 1 Telley, Agirman et al.

Fig. 1. Birthdate- and differentiation stage-related cellular diversity in the developing neocortex. (A) Schematic illustration of the experimental procedure. M-phase APs were labeled by FT injection performed at either E12, E13, E14 or E15 and isochronic cohorts of APs and daughter cells were collected either 1, 24 or 96 hours later. (B) t-SNE representation of the single cell RNA sequencing dataset revealing the transcriptional organization of the cells according to the time at which they were collected (*i.e.* their differentiation status) and the day on which the injection was performed (*i.e.* their birthdate). APs, BPs and Ns can be distinguished by their combinatorial expression of key marker genes (n = 20 transcripts). (C) Cluster analysis reveals transcriptionally distinct and temporally dynamic cellular clusters. Cluster nomenclature reflects prevalence of the cluster at a given embryonic age (early: E12/E13, late: E14/E15). Cells in these clusters express classical layer and cell-type marker genes in accordance with their birthdate and differentiation status. (D) Expression of the top 10 most enriched genes per cluster highlights cellular diversity. See also data table S1. (E) Spatio-temporal expression of cluster-specific transcripts with *in situ* hybridization. (ISH), from the Allen Developing Mouse Brain Atlas. Color-coded images represent the average expression for representative transcripts (see also figs. S2 and S3). Abbreviations: AP: apical progenitors, Astro: astrocyte, BP: basal progenitors, CP: cortical plate, IN: interneurons, N: neurons, N1d: 1-day-old neurons, N4d: 4-day-old neurons, VZ: ventricular zone, SVZ: subventricular zone.

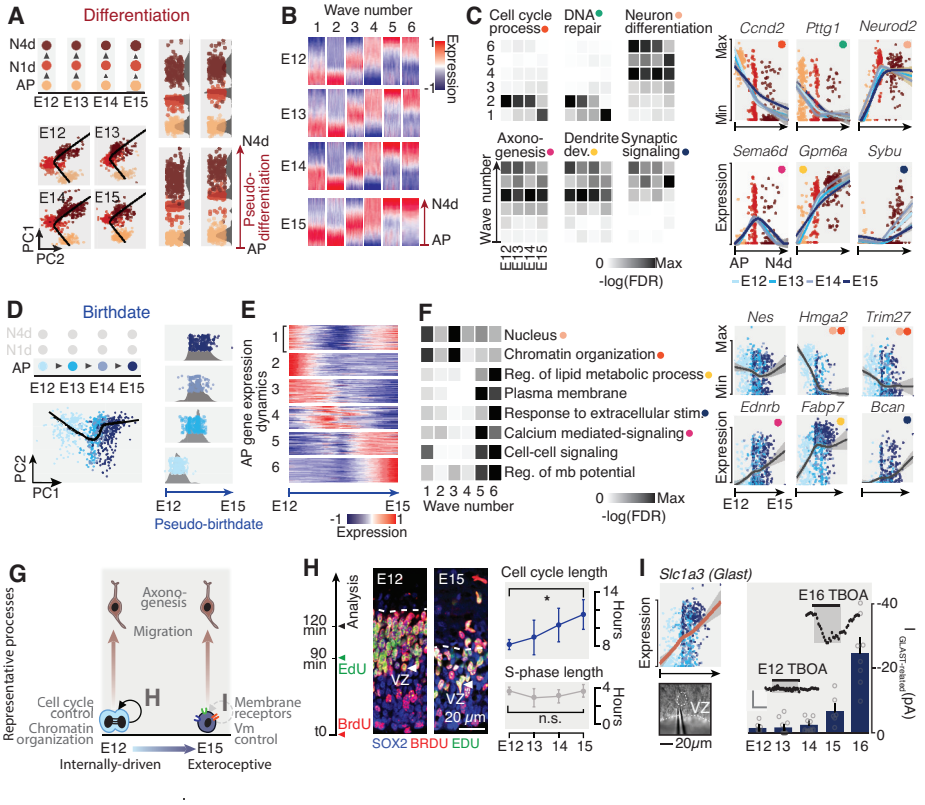

Figure 2 Telley, Agirman et al.

Fig. 2. Neuronal differentiation programs are conserved while APs shift from internally-driven to exteroceptive transcriptional states. (A) Principal component analysis (PCA) showing spontaneous organization of cells along a differentiation axis (*i.e.* from AP to N1d to N4d). Black line indicates pseudo-differentiation axis onto which cells were aligned. (B) Clustering of gene expression kinetics reveals sequential transcriptional waves. (C) Examples of gene ontology processes associated with each of the expression waves, along with sample corresponding genes. Note conserved dynamics across embryonic ages. See also fig. S5 and data tables S2 and S3. (D) PCA of AP transcriptional identity showing chronotopic organization along a birthdate axis (*i.e.* from E12 to E15). (E) Cluster analysis reveals distinct dynamics of AP gene expression during corticogenesis. (F) Examples of gene ontology terms associated with each expression dynamics, along with select corresponding genes. See also fig. S6 and data tables S4 and S5. (G) Schematic summary of the findings. (H) APs cycle progressively more slowly as corticogenesis unfolds. (I) The glutamate transporter transcript *Slc1a3* (*Glast*) is expressed by APs late in corticogenesis. Blockade of GLAST with TBOA (*35*) increases extracellular glutamate at late but not early embryonic ages, as detected by activation of ionotropic glutamate receptors in patch-clamped APs. Scale bars: 5 min; 20 pA. Abbreviations: AP: apical progenitor, CP: cortical plate, IZ: intermediate zone, N1d: 1-day-old neuron, N4d: 4-day-old neuron, PC: principal component, SVZ: subventricular zone, VZ: ventricular zone. * P <0.05, Student's t-test.

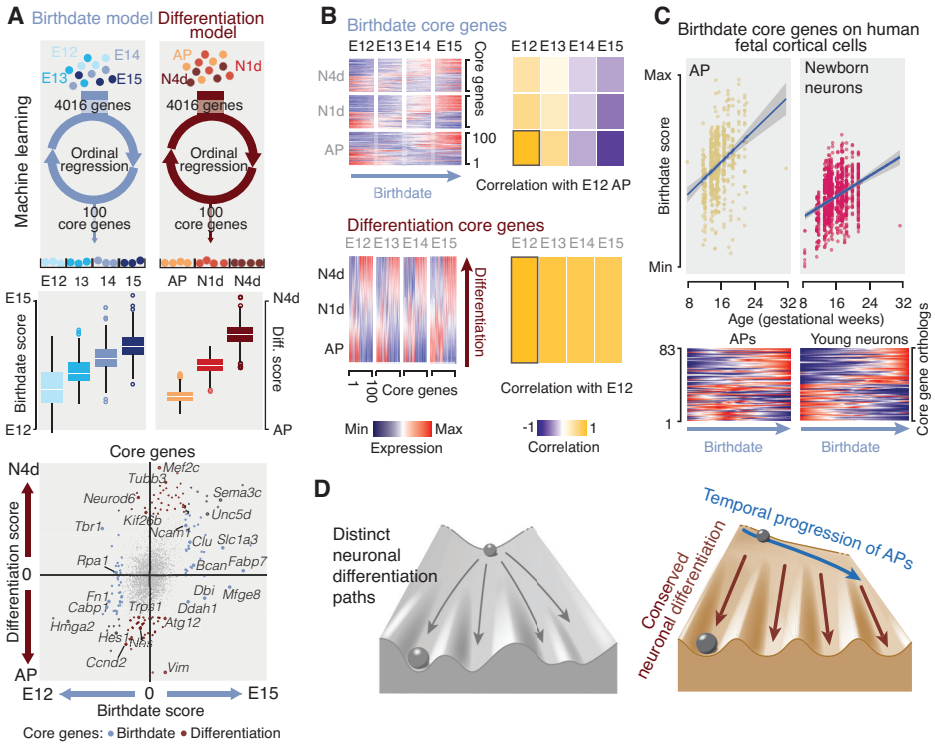

Figure 3 Telley, Agirman et al.

Fig. 3. Temporally progressing AP transcriptional states interact with conserved differentiation programs to generate neuronal diversity. (A) Machine learning approach used to identify a core set of genes which can classify cells based on their date of birth (top left) and differentiation status (top right). Center: Model performance using actual dataset. Box plot: median ± SEM. Bottom: Weight of the core genes in predicting birthdate and differentiation status. See also tables S1 and S2, and data table S6. (B) Top: Birthdate-associated core genes are temporally dynamic and daughter cells acquire embryonic stage-specific transcriptional birthmarks. See also Supplementary Fig. 7D. Bottom: In contrast, differentiation status-associated core genes are conserved across corticogenesis. (C) The transcriptional dynamics of the core gene orthologs (top) and the corresponding temporal patterning of daughter neurons and their mother cells (bottom) are conserved in human embryonic neocortex (dataset from ref.(*7*)) (D) Schematic representation of the findings: in the classical Waddington epigenetic model (left) cellular diversity emerges through distinct developmental trajectories. Right: the current data shows that instead, in the neocortex, developmental trajectories are conserved, but that initial ground states are temporally dynamic. Abbreviations: AP: apical progenitor, N1d: 1-day-old neuron, N4d: 4-day-old neuron.

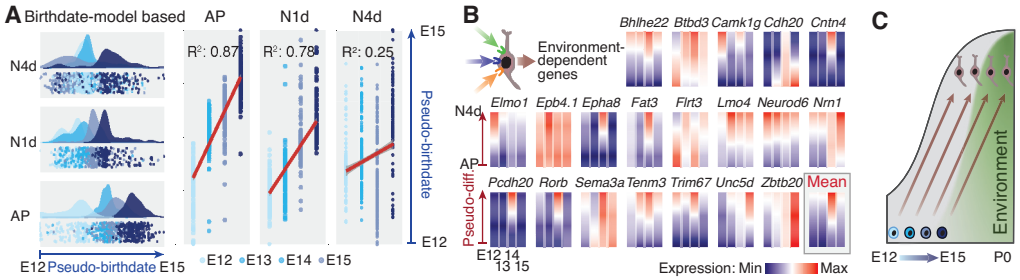

Figure 4 Telley, Agirman et al.

Fig. 4. Temporal birthmarks fade with differentiation as environment-dependent programs are implemented. (A) Pseudotime alignment of APs, N1d and N4d using the birthdate core genes presented in Fig. 3 reveals an overall fading of temporal birthmarks as neurons differentiate particularly affecting E14-born, L4-fated neurons. (B) Environment-dependent genes from ref. (*37*) are progressively upregulated in differentiating L4 neurons. (C) Schematic summary of the findings. Abbreviations: AP: apical progenitor, N1d: 1-day-old neuron, N4d: 4-day-old neuron.

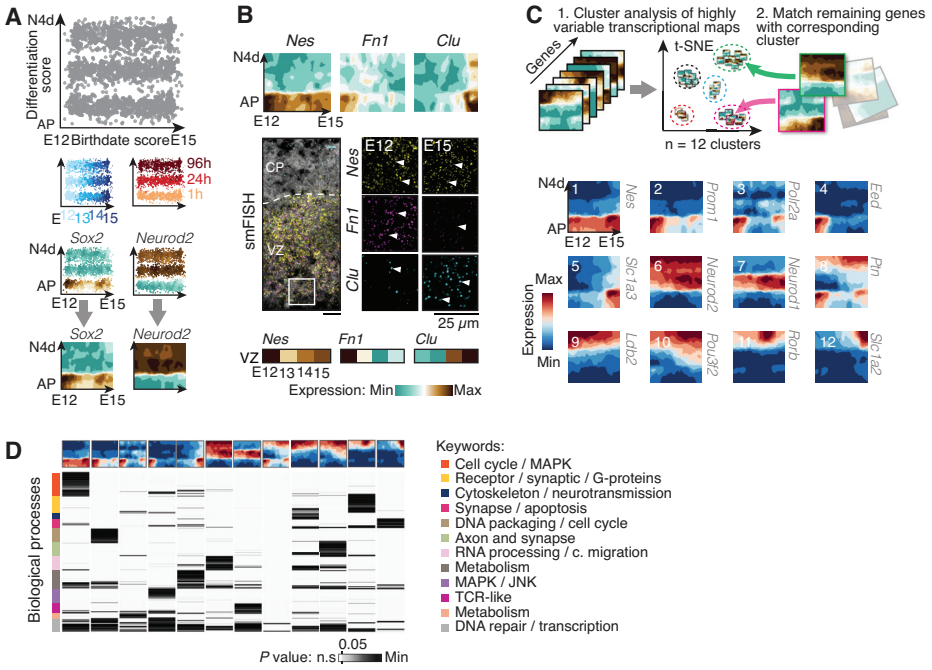

Figure 5 Telley, Agirman et al.

Fig. 5. Dynamic transcriptional mapping of corticogenesis. (A) Cellular map in which cells are displayed based on their combined expression of the core genes of the birthdate and differentiation status presented in Fig. 3. Dynamic expression of genes ("transcriptional maps") throughout corticogenesis can be determined based on this template (as exemplified with *Sox2* and *Neurod2*). (B) Example of transcriptional landscapes for select genes, and corresponding validation using smFISH. See also fig. S9A-C. (C) Canonical transcriptional maps can be identified by t-SNE clustering of the maps of individual genes. See also data table S7. See http://genebrowser.unige.ch/telagirdon/ for transcriptional maps for all expressed genes. (D) Genes belonging to each of the clusters have converging and specialized ontologies. See also data table S8. Abbreviations: AP: apical progenitor, N4d: 4-day-old neuron.

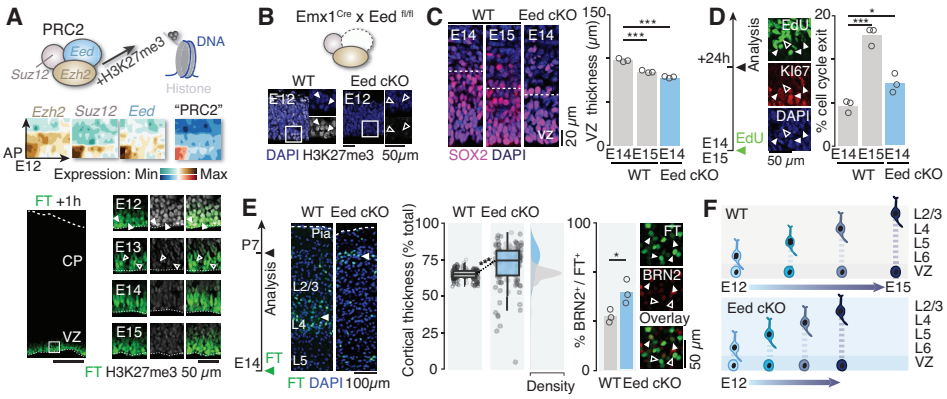

Figure 6 Telley, Agirman et al.

Fig. 6. PRC2 regulates the progression of AP temporal identity. (A) Top: the expression of the main subunits of the PRC2 complex is restricted to early APs. Bottom: the methylation mark of PRC2 has a corresponding temporal pattern. Dotted line indicates pial surface. (B) PRC2 function is disrupted in Eed cKO cortex, as shown by loss of the signature H3K27me3 mark. (C) VZ thickness is precociously decreased in Eed cKO cortex. (D) Cell cycle exit is precociously decreased in Eed cKO cortex. (E) The laminar position and molecular identity of E14-born, FT pulse-labeled neurons in Eed cKO cortex is shifted towards that of normally later-born neurons. (F) Schematic summary of the findings. Abbreviation: AP: apical progenitors, cKO: conditional knockout, CP: cortical plate, FT: Flashtag, N4d: 4-day-old neuron, PRC2: Polycomb Repressive Complex 2, VZ: ventricular zone, WT: wild-type. * P <0.05, *** P <0.0001, Student's t-test.

Table S1. Functional relevance of select core birthdate-related genes.

Table S2. Functional relevance of select core differentiation stage-related genes.

Science
AAAS

Supplementary Materials for

Temporal patterning of apical progenitors and their daughter neurons in the developing neocortex

L. Telley, G. Agirman, J. Prados, N. Amberg, S. Fièvre, P. Oberst, G. Bartolini, I. Vitali, C. Cadilhac, S. Hippenmeyer, L. Nguyen, A. Dayer, D. Jabaudon

Correspondence to: denis.jabaudon@unige.ch , ludovic.telley@unil.ch

This PDF file includes:

Other Supplementary Materials for this manuscript include the following:

Materials and Methods

Mice

All experiments were approved by the Geneva Cantonal Veterinary Authorities, Switzerland and the Austrian Federal Ministry of Science and Research in accordance with the Austrian and EU animal laws. CD1 WT mice were purchased from Charles River Laboratories and the embryonic day (E) 0 (three-hour time-mated females) or E0.5 (overnight-mated females) was established as the time of detection of the vaginal plug. In addition, the *Eed-flox* allele (*49*), *Emx1*-Cre (*50*) were used. MADM-*GT* and -*TG* cassettes (Chr. 7) were present in these lines (*51*) but this feature was not used here; the genetic background for these lines was mixed C57/Bl6, CD1. Both female and male embryos were analyzed in this study.

Genotyping of transgenic mice

Biopsies were collected and DNA extraction and PCR amplification were performed using the Phire Animal Tissue Direct PCR Kit (Thermo Scientific, #F-140WH) and following manufacturer's instructions. The following primers (5'-3') were used: Eed for - GGG ACG TGC TGA CAT TTT CT; Eed rev - CTT GGG TGG TTT GGC TAA GA; Cre for - GTC CAA TTT ACT GAC CGT ACA CC; Cre rev - GTT ATT CGG ATC ATC AGC TAC ACC. $Cre^{+}/Eed^{+/+}$ animals were used as WT, and $Cre^{+}/Eed^{fl/fl}$ as Eed cKO.

In utero FlashTag injection

FlashTag (FT) injections were performed between E12 and E15, as previously described (*13*). Briefly, pregnant females were anaesthetized with isoflurane, treated with Temgesic (Reckitt Benckiser, Switzerland) and the uterine horn was exposed following an abdominal incision. Half a microliter of 10 mM of a carboxyfluorescein succinimidyl ester (*i.e.* FlashTag, CellTrace™ CFSE, Life Technologies, #C34554) was injected into the lateral cerebral ventricle of the embryos. The abdominal wall was then closed and the embryos were let to develop until collection.

Immunofluorescence

Tissue processing: Embryonic brains were dissected in a phosphate-buffered saline (PBS) solution, fixed in 4% paraformaldehyde (PFA) overnight at 4°C then cryoprotected in PBS-sucrose

30% overnight at 4°C before embedding in OCT and freezing on dry ice. Postnatal mice were perfused with 4% PFA, brains were dissected and post-fixed in 4% PFA overnight at 4°C then stored in PBS. Coronal brain sections were performed using either a cryostat (embryonic brains; 14 µm) or a vibrating microtome (postnatal brains; 70 µm).

Immunofluorescence on brain sections: Brain sections were incubated 30min at 85°C in citrate buffer solution and washed 3 times in PBS prior to a 1-hour incubation in blocking solution (10% horse serum - 0,5% Triton X-100 diluted in PBS) at room temperature. Slides were then incubated overnight at 4°C with primary antibodies. Next, slides were washed 3 times in PBS and incubated 2 hours at room temperature with respective secondary antibodies (1:500). When applied, EdU was revealed following the manufacturer's instructions using Click-it chemistry (Invitrogen). Finally, slides were mounted with Fluoromount (Sigma). In Fig. 6A, the H3K27me3 image intensity range was normalized to the brightest juxtaventricular VZ cells at each embryonic age.

Immunofluorescence on in vitro culture: cells were fixed in 4% PFA for 15 min, treated with 0.25% Triton X-100 for 20 min and blocked in 0.5% BSA, 0.25% Triton X-100 for 1 hour at room temperature. Primary antibody incubations were performed overnight at 4° C, and secondary antibody incubations were performed 1 hour at room temperature. Coverslips were mounted on slides using Fluoromount (Sigma).

Antibodies: rabbit anti-pH3 (1:300, Abcam, #AB5176), rat anti-BrdU (1:200, Abcam, #AB6326), goat anti-BRN2 (1:500; Thermo Scientific, #PA5-1904), rat anti-CTIP2 (1:500, Abcam, #AB18465), rabbit anti-FITC (1:500, Abcam, #AB19491), rabbit anti-H3K27me3 (1:500, Millipore, 07-449 or Diagenode, C15410195), mouse anti-KI67 (1:200, Abcam, #AB15580), mouse anti-SOX2 (1:200, Santa Cruz; sc-365823), rat anti-TBR2 (1:300, Invitrogen, #14-4875-82). Secondary antibodies were used at 1:500 (Life Technologies).

Cell cycle length

Cell cycle length experiment was conducted following previously published paradigm (*32*). Briefly, at t0 pregnant females were injected peritoneally with BrdU (10mg/ml; 50 µl/10g) then at t1h30 with EdU (5mg/ml; 50µl/10g) and at t2h embryos were collected.

At least 3 sections per brain at each stage were quantified. The cell-cycle and S-phase duration were determined as follow: S-phase = 1.5 x ($SOX2^+BrdU^+EdU^+$ / $SOX2^+EdU^-$); total cell cycle = S-phase x ($SOX2^+$/ $SOX2^+EdU^+$) (*32*).

Electrophysiology

Four hundred µm-thick coronal slices were prepared from E12.5, E13.5, E14.5, E15.5 and E16.5 CD1 mice embryos and kept 30 minutes at 33°C in artificial cerebrospinal fluid (aCSF) containing 125 mM NaCl, 2.5 mM KCl, 1 mM $MgCl_2$, 2.5 mM $CaCl_2$, 1.25 mM NaH_2PO_4, 26 mM $NaHCO_3$ and 11 mM glucose, saturated with 95% O_2 and 5% CO_2. Slices were then transferred in the recording chamber, submerged and continuously perfused with aCSF. The internal solution used for the experiments contained 140 mM potassium methansulfonate, 2 mM $MgCl_2$, 4 mM NaCl 0.2 mM EGTA, 10 mM HEPES, 3 mM Na_2ATP, 0.33 mM GTP and 5 mM creatine phosphate (pH 7.2, 295 mOsm). Cells in immediate proximity to the ventricular wall (i.e. putative APs) were patched and clamped at -70mV. A baseline stable holding current was first measured for 4 minutes, after which a 10-minute bath of 100 µM of the glutamate transporter antagonist $_{DL}$-TBOA (DL-*threo*-β -Benzyloxyaspartate) (*52*) was applied and finally washed out. TBOA-induced currents were blocked by application of 25 µM NBQX and 50 µM D-APV (data not shown), consistent with activation of ionotropic glutamate receptors by increased extracellular levels of Glu (*52*). Recorded currents were amplified (Multiclamp 700, Axon Instruments), filtered at 5kHz, digitalized at 20kHz (National Instrument Board PCI-MIO-16E4, IGOR WaveMetrics), and stored on a personal computer for further analyses (IGOR PRO WaveMetrics). The net amplitude of TBOA induced currents was determined after subtraction of baseline holding current.

In vitro experiments

Embryos were injected with FT at E12 or E15 and collected 1 hour or 4 days after injection in ice-cold HBSS (Gibco; #14175-053). The dorsal pallium was microdissected under stereomicroscopic guidance (Leica, #M165 FC) using a microscalpel. Tissue from 5-6 littermates was pooled and incubated in 400 µl TrypLE (Gibco; #12605-010) for 5 minutes at 37°C. TrypLE was inactivated by adding HBSS containing 0.1% BSA and the tissue was mechanically dissociated by pipetting 6-8 times the suspension with a 1 ml pipette. Cells were filtered through a 70 µm cell strainer, centrifuged (150 rpm, 5 minutes) and resuspended in FACS buffer (L15 medium, Gibco; #21083-

027, containing 2 mg/ml glucose, 0.1% BSA, 1:50 citrate phosphate dextrose, 10 units/ml DNase I and 1 µM $MgCl_2$). The top 10% brightest FT positive cells were sorted on an S3e Cell Sorter (BioRad) or a BD FACS Aria II flow cytometer (BD Biosciences) and collected in ice-cold FACS buffer. Sorted cells were centrifuged (150 rpm, 5 minutes) and resuspended either in Neurobasal media (Gibco; #21103-049, supplemented with 500 mM Glutamax-I, 2% of B27 (Gibco; 17504-044), and 1% of penicillin/streptomycin antibiotic) or DMEM/F12 (Gibco; #31331-028, supplemented with 1× N2, Gibco; #A13707-01, FGF2; Sigma; #SRP4038-50UG, 2% of B27, and 1% of penicillin/streptomycin antibiotic). Sorted cells were plated on previously coated coverslips with poly-L-lysine (0.1mg/ml) and laminin (0.33µg/ml). Cells were maintained at 37° C with 5% CO_2 for 2 hours (*in vivo* arm) or 4 days *in vitro*. Following BRN2 and CTIP2 immunostaining, cells were imaged and the fluorescence intensity in the nucleus was calculated for both markers using R software. Cells with an intensity value for both markers below 25% to the maximum intensity per condition and cells with saturated intensity values for both markers were not considered for analysis. To mitigate potential artefactual staining, the thresholds were determined based on the *in vivo* condition: for the quantifications in fig. S8B, cells with a CTIP2/BRN2 ratio above 2.5 were considered as $CTIP2^+$ while cells with a CTIP2/BRN2 ratio below 1 were considered as $BRN2^+$.

Cell cycle exit

Pregnant females at E14.5 or E15.5 were injected i.p by a single pulse of EdU (1mg/ml; 50µl/10g) and embryos were collected 24 hours later. At least 3 sections per brain in each condition (n = 3 brains/condition) were quantified. The cell cycle exit rate was determined by dividing the number of $KI67^+EdU^+$ by the total number of EdU^+ cells.

Sm-FISH

Twelve µm-thick coronal sections were prepared from fresh frozen embryonic brains at E12, E13, E14 and E15 and incubated at room temperature for 1 hour. Sections were then fixed with 4% PFA for 15 min and processed according to the manufacturer's instructions, using the RNAscope Multiplex Fluorescent kit (Advanced Cell Diagnostics) for fresh frozen tissue. Briefly, sections were dehydrated using 50%, 70% and 100% successive baths. A 10 min treatment in SDS (4% in 200 mM sodium borate) was added in the protocol after Protease IV incubation as proposed in (*9*).

Fn1 (Channel 1), *Clu* (Channel 2), *Nes* (Channel 3) probes were then incubated on sections during 2 hours at 40°C and processed for amplification steps. Finally, sections were counterstained with DAPI and mounted with Mowiol medium. The following probes were used: *Nes* (Acdbio, #313161-C3), *Fn1* (Acdbio, #316951-C2) and *Clu* (Acdbio, #427891). For quantifications, images were processed using a custom script that identifies each molecule of mRNA and transformes it as a pixel. Pixels were then automatically counted in the VZ (delineated by the expression of Nestin mRNA). Three embryos per age were analyzed.

Imaging

Images were acquired using a LSM 700 confocal laser scanning microscope (Carl Zeiss), a Nikon A1r spectral line scan confocal or an inverted LSM800 confocal microscope (Carl Zeiss). For brain sections, the putative primary somatosensory (S1) cortex was used as a region of study. The Zeiss Zen Blue, ImageJ, Photoshop (Adobe) and R softwares were further used for downstream image processing and analyses.

Quantifications

In fig. S1B top, % $SOX2^+KI67^+/FT^+$ was calculated, with an $n = 3$ for each stage. Values ± SEM are: E12: 98.6 ± 1.5; E13: 96.2 ± 1.9; E14: 98.9 ± 1.11; E15: 98.6 ± 1.11. In fig. S1B bottom, % $TBR2^+KI67^+/TBR2^+$ was calculated. Values ± SEM are: E12: 71.7 ± 6.3; E13: 79.2 ± 7.5; E14: 56.0 ± 17.5; 16.8 ± 5.9.

In Fig. 2H, S-phase and total cell cycle length were calculated as mentioned above, with an $n = 3$ for each stage. For S-phase, values ± SEM are: E12: 4.3 ± 0.24; E13: 3.5 ± 0.6; E14: 3.7 ± 0.4; E15: 4.3 ± 0.4. For total cell cycle length, values ± SEM are: E12: 8.6 ± 0.3; E13: 9.4 ± 1.11; E14: 10.8 ± 1.1; E15: 12.0 ± 1.0. The values ± SEM for the fraction of S-phase APs in fig. S9C are: E12: 49.5 ± 1.1; E15: 35.7 ± 0.6.

In Fig. 2I, the net amplitude of GLAST-induced current was calculated. Values ± SEM are: E12: 1.6 ± 0.8 ($n = 6$); E13: 1.2 ± 0.8 ($n = 10$); E14: 2.6 ± 0.9 ($n = 8$); E15: 6.7 ± 2.4 ($n = 6$); E16: 24.8 ± 4.6.

In fig. S8B, % of $BRN2^+$ and $CTIP2^+$ cells were calculated as mentioned above. For the *in vivo* dataset (E12 $n = 2$; E15 $n = 3$), values ± SEM are: E12, $BRN2^+$: 88.1 ± 7.0; E12, $CTIP2^+$: 11.9 ±

7.0; E15, BRN2$^+$: 99.8 ± 0.1; E15, CTIP2$^+$: 0.40 ± 0.03. For the *in vitro* dataset (n = 3 per stage), values ± SEM are: E12, BRN2$^+$: 92.0 ± 6.2; E12, CTIP2$^+$: 12.1 ± 8.1; E15, BRN2$^+$: 99.6 ± 0.4; E15, CTIP2$^+$: 1.3.

In Fig. 6A (H3K27me3 staining) the H3K27me3 image intensity range was normalized to the brightest juxtaventricular VZ cells at each embryonic age. In Fig. 6C, VZ thickness delimited by the SOX2 staining was calculated (n = 3 brains per condition). Values ± SEM are: E14 WT: 97.8 ± 1.2; E14 Eed cKO: 78.5 ± 0.6; E15 WT: 84.7 ± 0.9.

In Fig. 6D, cell cycle exit rate was calculated as mentioned above (n = 3 brains per condition). Values ± SEM are: E14 WT: 6.2 ± 0.6; E14 Eed cKO: 9.5 ± 0.8; E15 WT: 17.0 ± 1.0.

In Fig. 6E, % of BRN2$^+$/FT$^+$ cells was calculated (n = 3 brains per condition). Values ± SEM are: WT: 36.8 ± 2.6; Eed cKO: 53.4 ± 4.8.

In situ hybridization image processing

All *in situ* hybridizations were retrieved from the Allen Developing Mouse Brain Atlas (www.brain-map.org) and uniformly zoomed to the putative S1 neocortical region. For the illustrations in Fig. 1E and figs. S2, S3, S6C and S7C, the images were aligned and stacked. The mean intensity level of the Z projection was calculated on ImageJ and the resulting layout was artificially colored using the "Fire" mode of ImageJ. In fig. S6C, semi-quantifications were performed by assigning a score to the strength of the signal in the juxtaventricular VZ (0 = absent, 1 = weak, 2 = medium, 3 = strong) for each gene. Genes were then grouped into early (*i.e.* belonging to dynamics 1-3) or late (*i.e.* belonging to dynamics 4-6) dynamics types and scores were averaged and normalized to the highest value across embryonic age. This scoring was performed blindly with regard to the gene identity.

scRNAseq experiment

Cell dissociation and FAC-sorting: Pregnant females were sacrificed either 1, 24 or 96 hours after FT injection. As previously described (*13*), embryonic brains were extracted in ice-cold HBSS, embedded in 4% agar low-melt and sectioned coronally at 300 µm using a vibrating microtome (Leica, #VT100S). The putative S1 cortical region was microdissected under a stereomicroscope and incubated in 0.05% trypsin at 37°C for 5 minutes. Following tissue

digestion, fetal bovine serum was added to the mix and cells were manually dissociated via up-and-down pipetting. Cells were centrifuged 5 min at 300 G and the pellet was suspended in 1 ml of HBSS then passed on a 70 µm cell strainer. FT^+ cells, gated to include only the top 5% brightest cells (*12,13*), were finally FAC-sorted on a MoFloAstrios device (Beckman).

Single-cell RNA capture and sequencing: FAC-sorted FT^+ cells (18 µl) were mixed with the C1 Suspension Reagent (2 µl; Fluidigm) yielding a total of 20 µl of cell suspension mix with ~500 cells / µl. The cell suspension mix was loaded on a C1 Single-Cell AutoPrep integrated fluidic circuit (IFC) designed for 10- to 17-µm cells (HT-800, Fluidigm #100-57-80). Batch effects were mitigated by distributing cells in the different conditions within single chips (*i.e.* E12 with E14 and E13 with E15) and by normalizing the number of reads per chip. cDNA synthesis and preamplification was processed following the manufacturer's instructions (C1 system, Fluidigm) and captured cells were imaged using the ImageXpress Micro Widefield High Content Screening System (Molecular Devices®). Single cell RNA-sequencing libraries of the cDNA were prepared using Nextera XT DNA library prep kit (Illumina). Libraries were multi-plexed and sequenced according to the manufacturer's recommendations with paired-end reads using HiSeq2500 platform (Illumina) with an expected depth of 1M reads per single cell, and a final mapping read length of 70 bp. All the single cell RNA capture and sequencing experiments were performed within the Genomics Core Facility of the University of Geneva.

The sequenced reads were aligned to the mouse genome (GRCm38) using the read-mapping algorithm TopHat. Unique Molecular Identifiers (UMI) sequenced in the first reads were used to correct for cDNA PCR amplification biases. Duplicated reads were identified and corrected using the deduplication step from the UMI-tools algorithm (*53*). The number of reads per transcript was calculated with the open-source HTSeq Python library. All the analyses were computed on the Vital-It cluster administered by the Swiss Institute of Bioinformatics.

scRNAseq analysis

Cell filtering: Doublet cells identified on the Fluidigm C1 plate images were excluded before initial analysis. A total of 2,906 FT^+ single cells were obtained (**FT^+1 h**: E12: 202 cells, E13: 211, E14: 135, E15: 304; **FT^+24 h:** E12: 284 cells, E13: 286, E14: 232, E15: 217; **FT^+ 96 h:** E12: 246 cells, E13: 278, E14: 262, E15: 249). Cells expressing < 1000 genes or > 17% of mitochondrial genes were excluded. After this step, 2,756 cells remained for analysis (**FT^+1 h**: E12: 189 cells,

E13: 207, E14: 134, E15: 301; **FT $^{+}$24 h:** E12: 268 cells, E13: 223, E14: 219, E15: 213; **FT $^{+}$96 h**: E12: 244 cells, E13: 267, E14: 254, E15: 237).

Type specific transcripts: The AP, BP and N score used in Fig. 1B correspond to the mean transcript expression of the top 20 genes for AP, BP and N previously characterized in (*12*) were: **AP**: *Aldoc, Pdpn, Vim, Ednrb, Ddah1, Ldha, Peg12, Wwtr1, Tspan12, Mfge8, Uhrf, Ncaph, Ndrg2, Mt1, Hk2, Psat1, Sp8, Sdc4, Dnmt3a, Notch2, Psph*. **BP**: *Btg2, Eomes, Abcg1, Kif26b, Mfap4, Coro1c, Myo10, Mfng, Rprm, Chd7, Ezr, Gadd45g, Slc16a2, Heg1, Celsr1, Tead2, Cd63, Rhbdl3, Mdga1, Arrdc3*. **N**: *Myt1l, Unc5d, 1700080N15Rik, Nos1, Satb2, Ank3, Scn3a, Dscam, Cntn2, Plxna4, 9130024F11Rik, Lrrtm4, Ptprk, Nrp1, Celsr3, Rbfox1, Flrt2, Kcnq3, Kcnq2, Gm36988.*

Clustering analysis was performed using the Seurat bioinformatics pipeline (https://github.com/satijalab/seurat) and is summarized here. We first created a "Seurat object" including all 2,756 cells and all genes. To remove sequencing depth biases between cells, we normalized and scaled the UMI counts using the *NormalizeData* (normalization.method = "LogNormalize", scale.factor = 100000) combined with the *ScaleData* function (vars.to.regress = c("nGene","nUMI")). A cell cycle phase was further assigned to each single cell using the Seurat pipeline. Gene expression was not normalized with regard to the cell cycle phase as this process is physiologically relevant in the temporal progression of cortical progenitors identity. We then determined the most variable genes by plotting transcripts into bins based on X-axis (average expression) and Y-axis (dispersion). This identified 4,016 transcripts. Parameters and cutoffs were set as follow: mean.function = ExpMean, dispersion.function = LogVMR, x.low.cutoff = 0.1, x.high.cutoff = 8, y.cutoff = 0.7. Next, we identified the statistically significant principal components and used the top 20 as input for t-Distributed Stochastic Neighbor Embedding dimensional reduction, using the *TSNEPlot* function. To identify cellular clusters, we adopted a graph-based clustering approach using *FindClusters* function with a 1.8 resolution. Finally, a multiclass SVM model (implementation from R package *bmrm*) was trained on all cluster. The robustness of the clustering was validated using an in-silico downsampling approach. Briefly, cells were randomly sampled down and re-clustered and the stability of the cellular cluster was estimated, and compared to a random clustering. Finally, a multiclass SVM model (implementation from R package *bmrm*) was trained on all cluster- assigned cells and genes were ranked according to their linear weights. For each class (*i.e.* clusters), genes with a significant linear weight (Z-test, FDR ≤ 0.05) were considered as enriched genes.

Pseudotime projection: APs, N1d and N4d cells at all embryonic ages identified in the cell clustering analysis were processed. Basal progenitors were not included in this analysis because N1d and N4d are overwhelmingly directly born from APs when using FT labeling (*12,13*). The pseudotime alignment method performed was previously described (*24*) and is summarized hereafter. In Fig. 2 and figs. S5 and S6, we restricted the datasets to the high variable genes (n = 4,016) and performed dimensionality reduction using the prcomp function of R software. Taking into consideration the significant principal components (PCs) explaining at least 2% of the total variance and using the R package princurve, we fitted a curve that described the maturation route (*i.e.* pseudo-birthdate or pseudo-differentiation) along which cells are organized. The beginning of the curve was established as the side where cell expressing the highest level of *Sox2* (AP) for pseudo-differentiation or the highest level of *Hmga2* (E12) for pseudo-birthdate. A maturation score reflecting the distance beginning of the curve-cell coordinate was attributed to each cell and normalized between 0 to 1. This pseudotime alignment method was also validated on the AP population using the Monocle bioinformatic pipeline (*14*).We then restricted the dataset to the top 500 genes for each PCs and performed a "Partitioning Around Medoids" analysis using the PAM R package (K = 6, span = 0.6) and each gene expression dynamics was normalized between -1 and 1 to identify clusters of transcripts with similar dynamics along the pseudo-differentiation (Fig. 2A, fig. S5) or pseudo-birthdate (Fig. 2D, fig. S6). This approach was previously described elsewhere (*24*).

Ordinal regression models: We used a regularized ordinal regression method to predict on one hand the birthdate and on the other hand the differentiation status of each cell. We restricted the analysis to the high variable genes (n = 4,016) defined earlier. As the cells are expected to be organized within a differentiation and a birthdate continuum, we used and adapted a previously described ordinal regression model (*54*) implemented in the *bmrm* R package. In our context, a single linear model is optimized to predict cell differentiation status irrespectively of the date of birth and conversely. The linear weight of the models is used to rank the genes according to their ability to predict each cell category and the best 100 genes (top 50 and bottom 50) in each model were considered. The ordinal regression models were then re-optimized on these subsets of genes. In the ordinal regression model, the prediction scores are defined by the linear combination of the core genes expression. Since the values of the prediction score *per se* are arbitrary, the minimum and maximum values were replaced with AP / E12 and N4d / E15, respectively, in the

differentiation and birthdate models. All reported predictions were obtained by 10-fold cross-validation. For the birthdate prediction of the human embryo neocortical cell dataset (*7*), we first isolated APs and newborn neurons using the annotations provided by the authors. The dataset was then restricted to the human orthologs of the birthdate core genes identified in the current study and the pseudo-birthdate of these cells was calculated using the aforementioned birthdate ordinal regression model. The expression dynamics of the ortholog core genes were plotted along this pseudo-birthdate for both APs and their newborn progeny.

Transcriptional maps (Fig. 5): Cells were organized on a 2D grid based on their birthdate and differentiation status score. For this purpose, the data were linearly adjusted so that the average predicted values for each cardinal feature was aligned on to the relative knot of the grid. The gene expression at a given coordinate of the 2D space was further estimated as the average expression of its 15 nearest neighbors. All transcriptional landscapes of the most variable genes (n = 4,016) were further clustered by projecting genes onto a 2D t-SNE space and submitted to a k-means clustering (K = 12). The average expression pattern was calculated for each cluster and the transcriptional maps of all remaining genes (n = 12,425) were correlated to theses 12 patterns. Select examples in Fig. 5C correspond to genes directly assigned or highly correlated to corresponding cluster.

Softwares

All single cell RNA sequencing analysis were perfomed using the R software with publicly available packages. GeneGo portal (https://portal.genego.com) was used to investigate the enriched gene ontology processes in Fig. 2 and Fig. 3 and the biomart R package served to extract the list of genes allocated to a defined ontology term. Cytoscape platform (*55*) associated with its plugin (*56*) was used to construct the enrichment gene ontology processes network in supplementary fig. S10. For this purpose, the latest version of gene ontology (go-basic.obo) and gene association (gene_association.mgi) from the Gene Ontology Consortium website (www.geneontology.org) were given as input in Bingo. The string database (http://string-db.org) implemented in Cytoscape platform was used to determine the protein-protein interactions in figs S5, S6 and S7.

Table S1: Selection of characterized genes from the birthdate model

Gene symbol	Enriched in	Gene weight	Function	References (PMID)
Hmga2	Early	-6.25	DNA-binding, chromatin-related. KO in early-stage cortical progenitors reduces neurogenic potential	22797695 / 18957199
Tbr1	Early	-3.65	TF. Instructs the laminar location and identity of deep layer neurons	16858776 / 20615956
Top2a	Early	-3.36	DNA topoisomerase. KO leads to laminar dysruptions in the cerebral cortex	12773624
Bcl11b	Early	-3.13	CTIP2, a TF. Marker of L5B neurons	15664173 / 18678899
H2afz	Early	-2.91	Histone protein. KO results in enhanced proliferation of progenitors and reduced differentiation.	29294103
Gadd45g	Early	-2.78	DNA demethylation. Direct target of Pax6.	19521500
Hes1	Early	-2.58	Transcriptional repressor. Represses precocious neuronal commitment of cortical progenitors	10627606
Filip1	Early	-2.24	Filamin-interacting protein. Controls the radial migration of newborn cortical neurons	12055638
Sox5	Early	-2.15	TF. Control the timing of sequential generation of corticofugal neurons subtypes	18215621 / 18840685
Ptprz1	Late	2.73	Receptor tyrosine phosphatase. In human oRGs; development of OPCs.	26406371 / 21969550
Cttnbp2	Late	2.85	Dendritogenesis	23015759
Sparcl1	Late	2.88	Surface protein. Terminal migration of neurons. Astrocyte marker	14715135
Glra2	Late	2.91	Glycin receptor subunit. Regulates BP generation	24926615
Trim9	Late	3.02	Ubiquitin ligase. Netrin1 signaling-associated; regulates neuronal morphogenesis	28701345
Nr2f1	Late	3.09	TF, COUP-TFI. Neuronal differentiation	25476200
Trim2	Late	3.36	Regulates axonal mrophogenesis	20796172
Tnc	Late	3.86	Extracellular matrix protein. oRG marker	26406371
Chl1	Late	3.92	ECM and cell adhesion protein. Inhibits Erk1/2- MAPK signaling and reduces progenitor proliferation	15504324 / 20933598 / 18077678
Unc5d	Late	4.36	Netrin receptor. Expressed in L4 neurons; mediates neuronal survival	21216843 / 18469807
Sema3c	Late	5.36	Semaphorin. Required for migration of superficial layer neurons	26182416
Zbtb20	Late	7.04	Regulator for the generation of layer-specific neuronal identities; neuronal maturation	27282384 / 24828045

Table S2: Selection of characterized genes from the differentiation model

Gene symbol	Enriched in	Gene weight	Function	References (PMID)
Vim	AP	-4.85	Intermediate filament protein. Classical marker of radial glia cells	Multiple references
Ccnd2	AP	-3.43	Cylin D2. Required for generation of BPs from APs	19641124
Chd7	AP	-3.17	Chromatin remodeler. Regulates AP proliferation; interacts with Sox2	27955690 / 21532573
Boc	AP	-3.10	SHH co-receptor. Regulates neuronal differentiation from cortical progenitor cells	27871935
Cdon	AP	-3.07	SHH co-receptor. Regulates cortical progenitor proliferation and neuronal differentiation	16648472
H2afz	AP	-2.98	Histone protein. KO results in enhanced proliferation of progenitors and reduced differentiation.	29294103
Hes1	AP	-2.88	Transcriptional repressor. Represses precocious neuronal commitment of cortical progenitors	10627606
Nes	AP	-2.65	Intermediate filament protein. Classical marker of radial glia cells	Multiple references
Rapgef6	AP	-2.59	GTPase. Reported to maintain the apical surface adherens junction in cortical progenitors.	27390776 / 28917843
Bcl11b	AP	-2.55	CTIP2, a TF. Marker of L5B neurons	15664173 / 18678899
Nfia	AP	-2.51	TF. Represses Notch pathway to initiate neuronal differentiation	20610746
Hmga2	AP	-2.31	DNA-binding, chromatin-related. KO in early-stage cortical progenitors reduces neurogenic potential	22797695 / 18957199
Qk	AP	-2.30	Involved in neuron-glia fate decisions	9778149
Arx	AP	-2.11	TF. Regulates AP proliferation and generation of BPs	23968833 / 18509041
Unc5d	N	3.06	Netrin receptor. Expressed in L4 neurons; mediates neuronal survival	21216843 / 18469807
Aff2	N	3.08	TF, transiently expressed in SVZ. Reported role in lymphcyte differentiation	12079280
Sparcl1	N	3.10	SVZ protein; obligatory binding partner of the neurite outgrowth-promoting factor pleiotrophin	28823557
Syt4	N	3.23	Syntaxin 4, retrograde synaptic signalling	23522040
Celf2	N	3.25	Regulation of RNA splicing	11158314
Nlgn3	N	3.28	Neuroligin 3, synaptic adhesion molecule	26235839
Sox11	N	3.30	TF, interacts with LHX2	28053041
Trim67	N	3.36	KO has CNS defects including decreased size of callosum	26235839
Nrxn1	N	3.37	Neurexin 1, synaptic protein	28013231
Zbtb18	N	3.40	Disruption of superficial cortical layers in KO	28053041
Dkk3	N	3.52	Wnt pathway inhibitor	18719393
Dpysl3	N	3.56	Axonal guidance and outgrowth	10504203
Bcl11a	N	3.63	TF. Controls the migration of cortical neurons with Sema3c; settles identity of corticofugal neurons	26182416 / 25972180
Sema3c	N	3.76	Semaphorin. Required for migration of superficial layer neurons	26182416
Neurod6	N	3.88	TF. Classical neuronal marker	Multiple references
Satb2	N	3.88	TF. Regulates differentiation of callosal projection neurons; mutually repressive interactions with Fezf2	26324926 / 25037921 / 18255031/ 18255030
Dcx	N	3.98	Microtubule associated protein. Critical for neuronal migration and proper cortical layering	10399932 / 10399933 / 14625554 / 12764037
Clstn2	N	4.11	Excitatory synapse transmission	12498782 / 28912692
Tuba1a	N	4.11	Tubulin-related. Mutation causes lisencephaly	20466733
Arpp21	N	4.23	RNA-binding; controls neuronal excitability and dendritic morphology in neocortex	29581509
Gpm6a	N	4.34	Neuronal differentiation and migration of neuronal stem cells	19298174
Smarca2	N	4.37	Chromatin-remodeling; activation of *Neurod2* and *Ngn*	11134956 / 15576411
Rtn1	N	4.38	ER-related; involved in neuronal differentiation; used as a marker	9560466
Neurod2	N	4.46	Neuronal specific genes, induces premature exit from cell cycle	26940868
Zbtb20	N	4.51	Regulator for the generation of layer-specific neuronal identities; neuronal maturation	27282384 / 24828045
Gria2	N	4.57	AMPA receptor subunit	Multiple references
Tubb3	N	4.63	Tubulin-related. Mutation causes abnormal cortical development	30016746
Mef2c	N	5.37	Activity-dependent TF. Regulates synaptogenesis	27989458

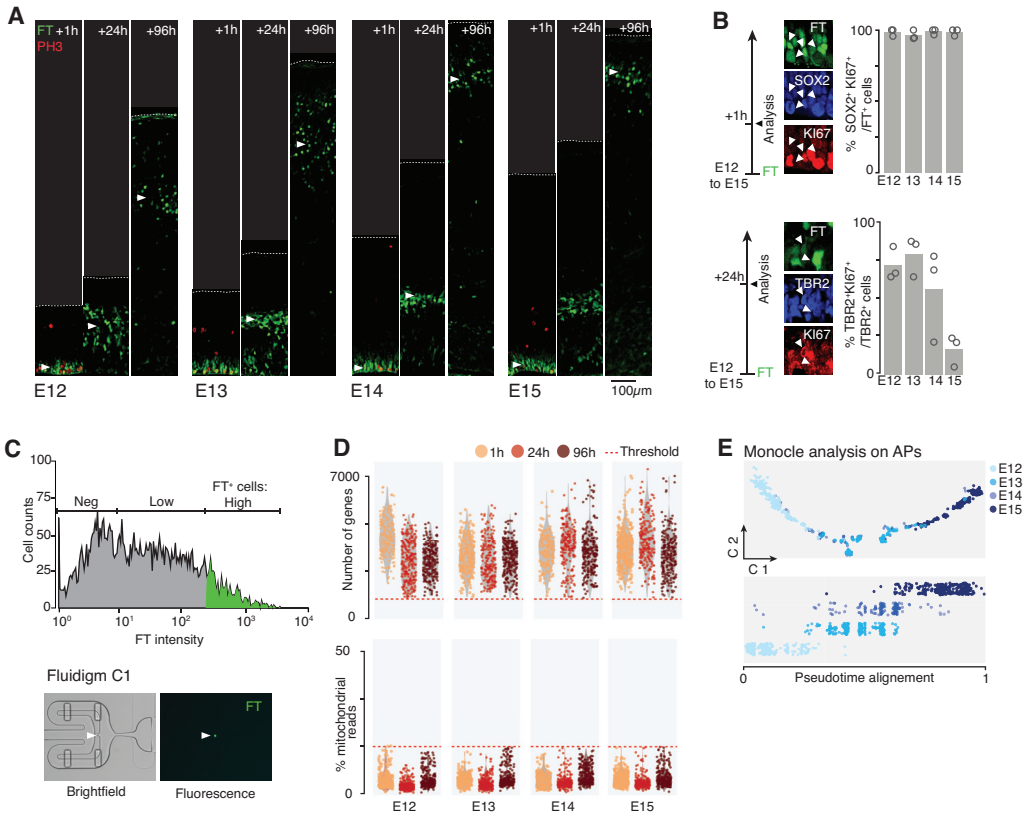

Fig. S1. scRNA sequencing of isochronic cohorts of cells in the developing neocortex. (A) FT injection labels isochronic cohorts of cortical cells which were collected either 1, 24 or 96 hours after labeling. E12 illustration modified from Fig.1. (B) Top: essentially all FT+ SOX2+ cells are proliferative (*i.e.* KI67+) at the FT+1h collection time point, throughout corticogenesis. Bottom: the fraction of proliferative TBR2+ cells (*i.e.* including intermediate progenitors) decreases with corticogenesis. (C) FT+ cells were FAC-sorted (top) and captured on a C1 microfluidic device (bottom) for scRNAseq processing. (D) Number of genes (top) and the percentage of mitochondrial genes (bottom) in each cell. Lower (< 1000 genes) and upper (> 17% mitochondrial genes) accepted thresholds are displayed. (E) Unbiased analysis of single-cell trajectories (Monocle) (14), highlighting the AP birthdate axis. Abbreviations: C: component, AP: apical progenitor, FT: Flashtag.

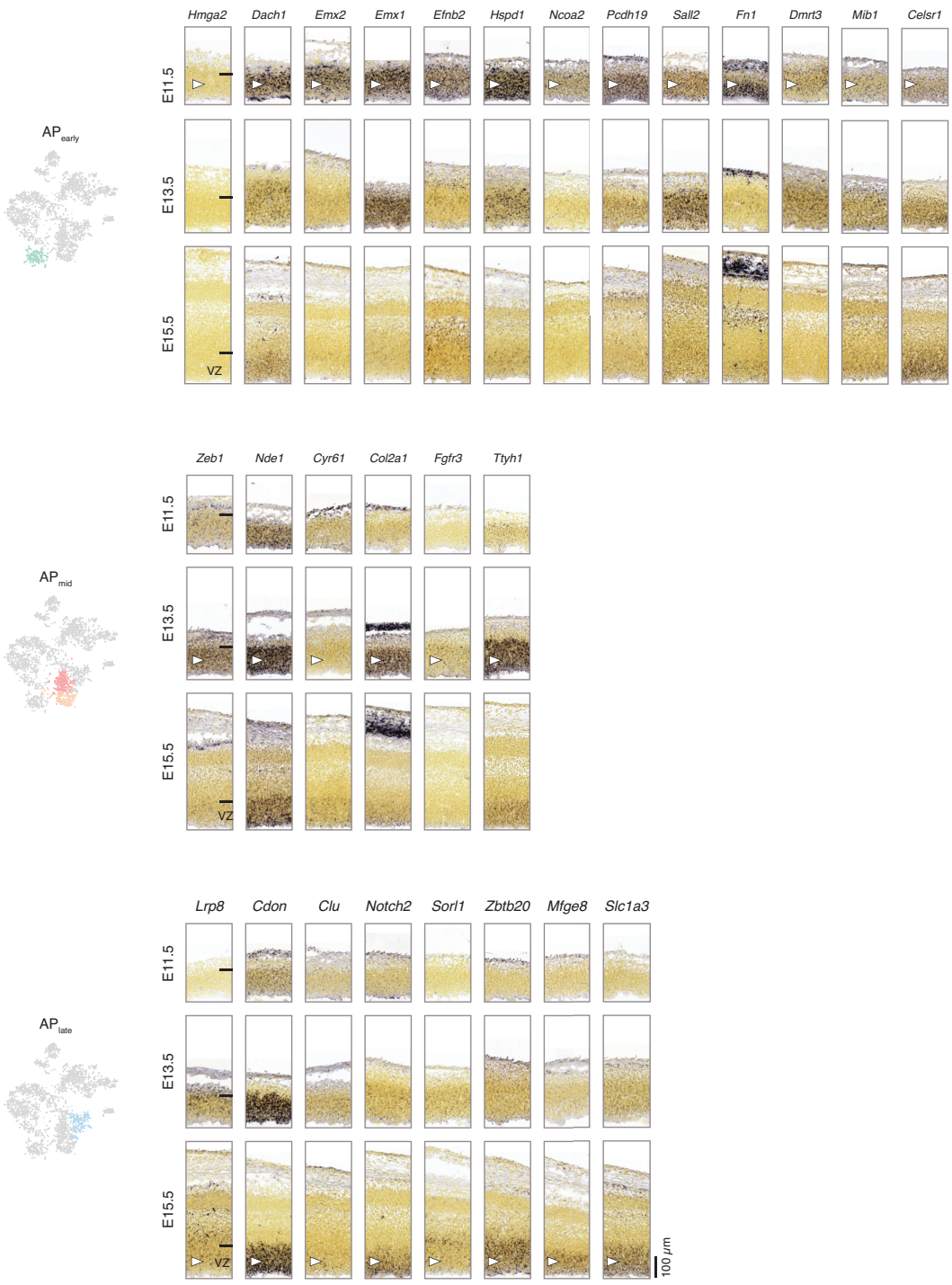

Fig. S2. Spatio-temporal expression of the most enriched genes in AP clusters. In situ hybridization of genes enriched in APearly, APmid, and APlate clusters. The ISH merged layouts are also presented in Fig. 1E. Tick mark indicates VZ basal border. Source of ISH: Allen Developing Mouse Brain Atlas. Abbreviations: AP: apical progenitor, VZ: ventricular zone.

Fig. S3. Spatio-temporal expression of the most enriched genes in 4-day-old clusters. Individual and merged in situ hybridization of genes enriched in N4dearly1, N4dearly2, N4dlate1 and N4dlate2 clusters. The ISH merged layouts for N4dearly1 and N4dlate2 are also presented in Fig. 1E. Source of ISH: Allen Developing Mouse Brain Atlas. Abbreviations: CP: cortical plate, N4d: 4-day-old neurons.

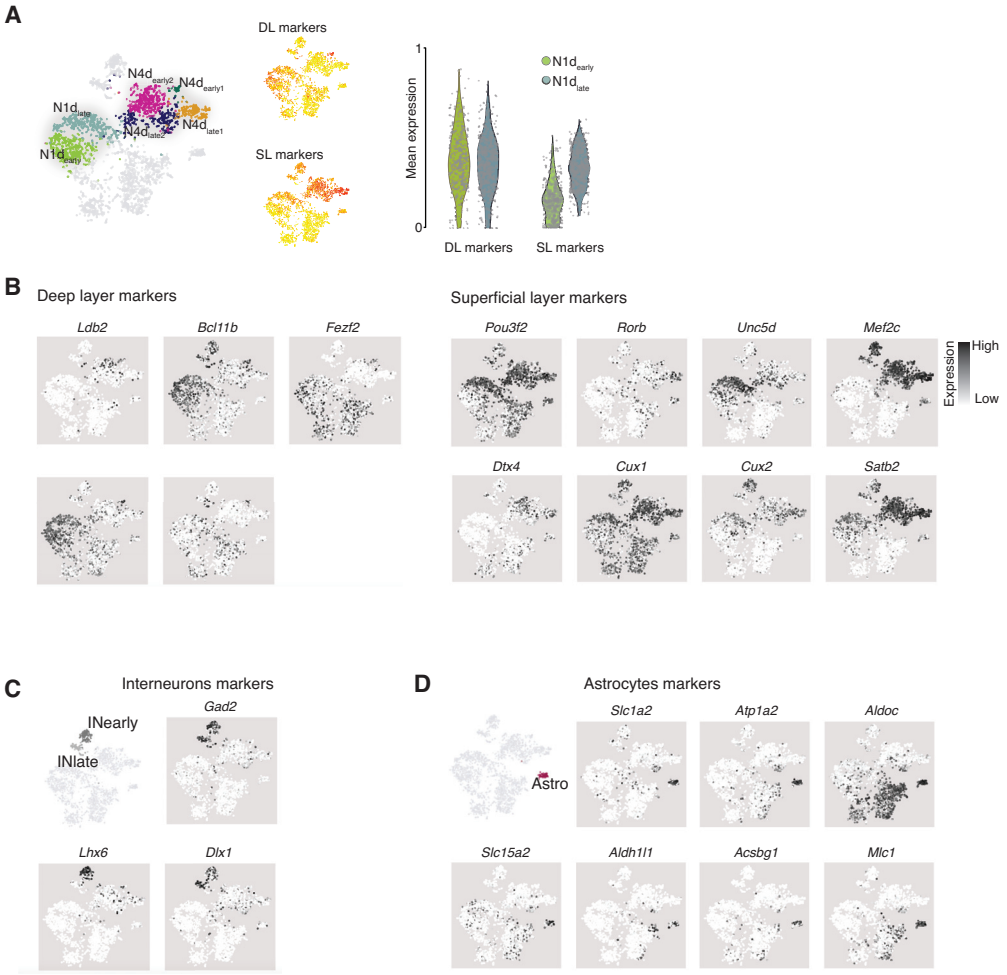

Fig. S4. Expression of select genes in neurons, astrocytes, and interneurons. (A) Feature plots showing expression of classical deep layer (DL) and superficial layer (SL) markers in 1-day and 4-day-old neurons across corticogenesis. Note that N1dlate neurons (*i.e.* E14 and E15-born neurons) initially and transiently express DL markers, as illustrated in the violin plots. (B) Expression of select laminar markers. (C) Expression of select astrocytes markers. (D) Expression of select ventral pallial-derived interneuron markers. Abbreviations: Astro: astrocytes, DL: deep layers, IN: interneurons, N1d: 1-day-old neurons, N4d: 4-day-old neurons, SL: superficial layers.

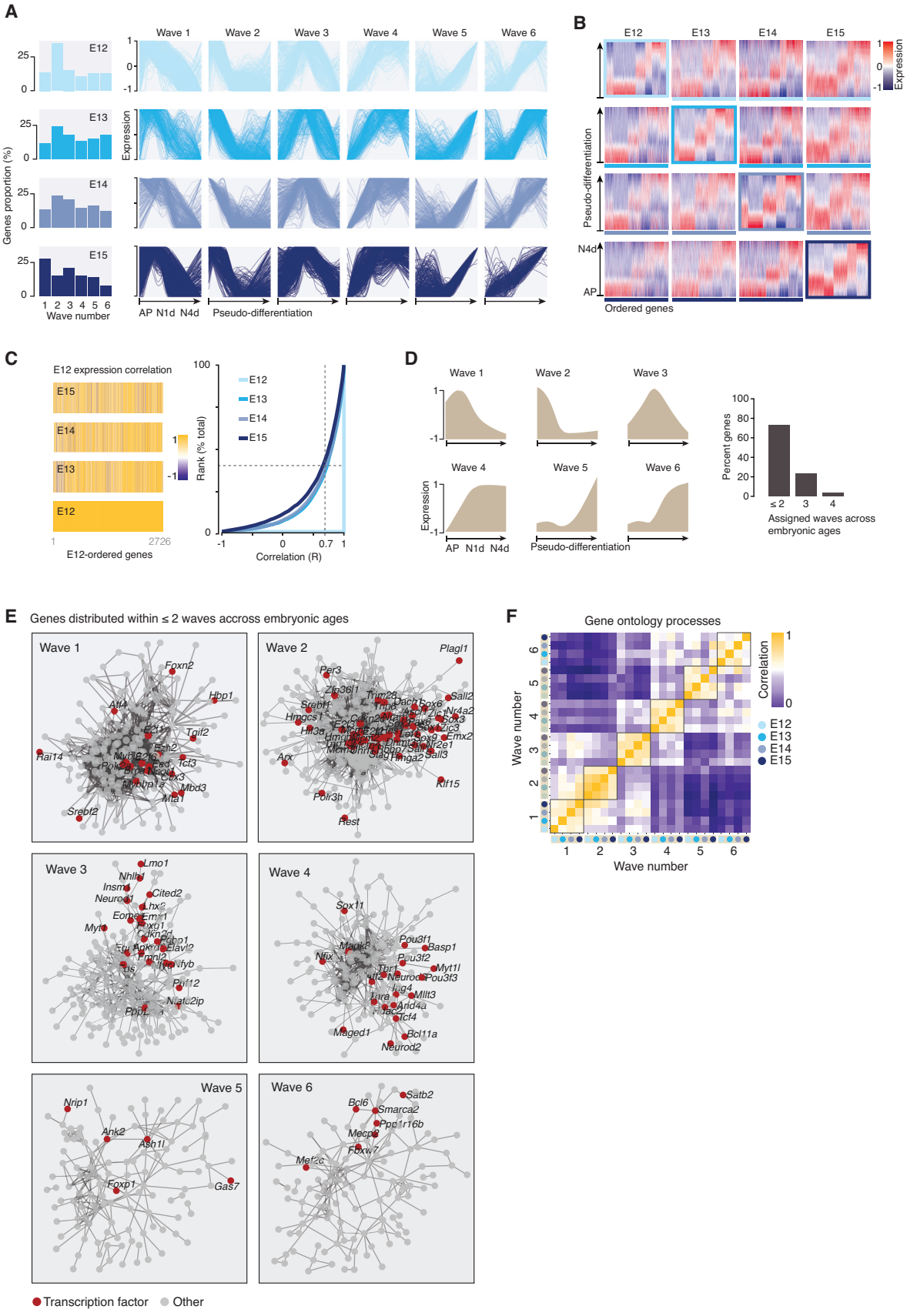

Fig. S5. Transcriptional differentiation waves at each embryonic age. (A) Gene distribution across the six differentiation waves at each embryonic age. (B) Gene waves at each embryonic age, organized by a reference E12 sequence. (C) Left: Correlation of gene kinetics considering E12 as a reference shows that most gene expression dynamics are independent of the developmental age. Right: About half of the expressed genes had highly conserved expression dynamics. (D) Gene distribution within waves across embryonic ages. (E) Protein-protein interactome (from https://string-db.org/) of the most stable gene within each wave. Unassigned genes are not displayed. (F) Parallel progression of gene ontology processes associated with each transcriptional wave. Abbrevations: AP: apical progenitor, N4d: 4-day-old neurons.

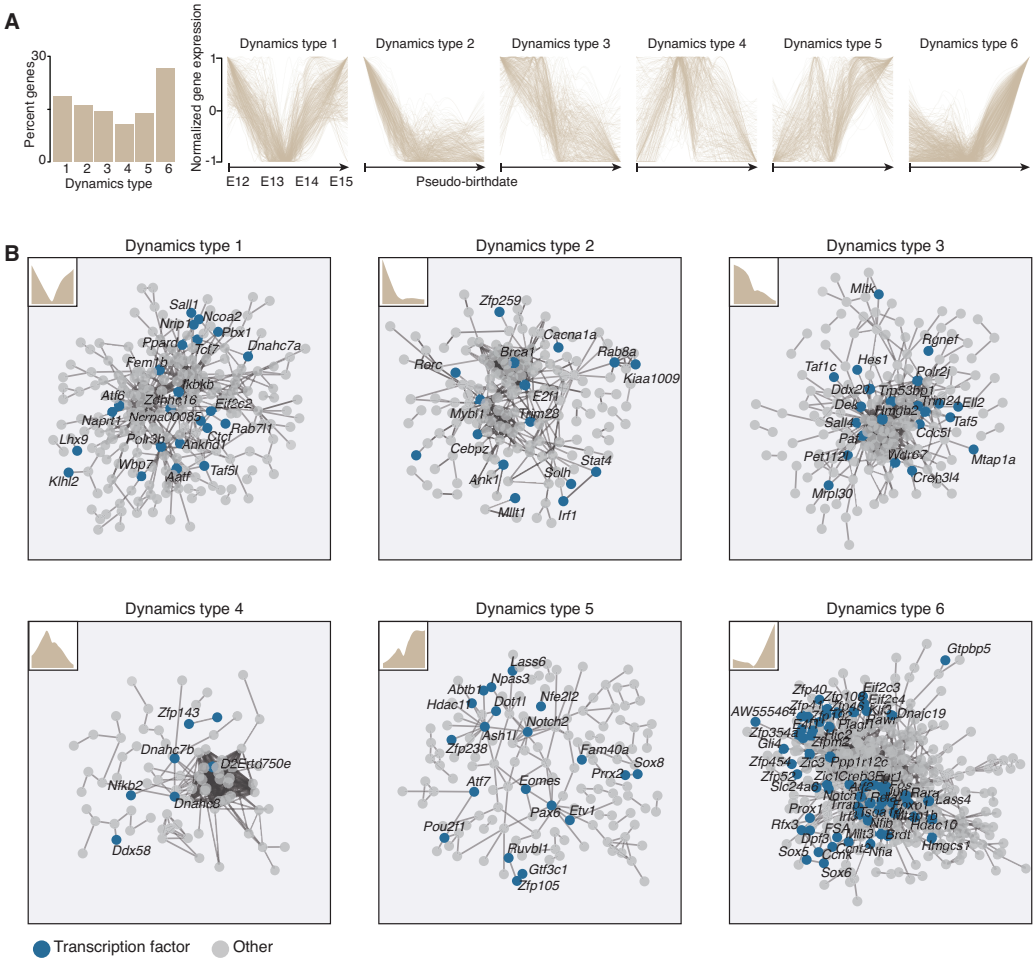

Fig. S6. Sequential AP transcriptional states across corticogenesis. (A) Normalized gene expressions are distributed within six sequential AP transcriptional states. (B) Global protein-protein interactome for each AP state, from https://string-db.org/. Unassigned genes are not displayed. (C) Sample and cumulative ISH hybridizations for all dynamically-expressed genes in the Allen Developing Mouse Brain Atlas. Righ: semi-quantifications of the ISH intensity in the VZ for the aggregate early (*i.e.* 1 to 3) and late (*i.e.* 4 to 6) dynamics. (D) The fraction of APs in G1 increases across corticogenesis as a result of the lengthening in the cell cycle, as reflected by expression of cell-cycle-enriched transcripts (see Methods for details). Abbreviation: AP: apical progenitor, VZ: ventricular zone.

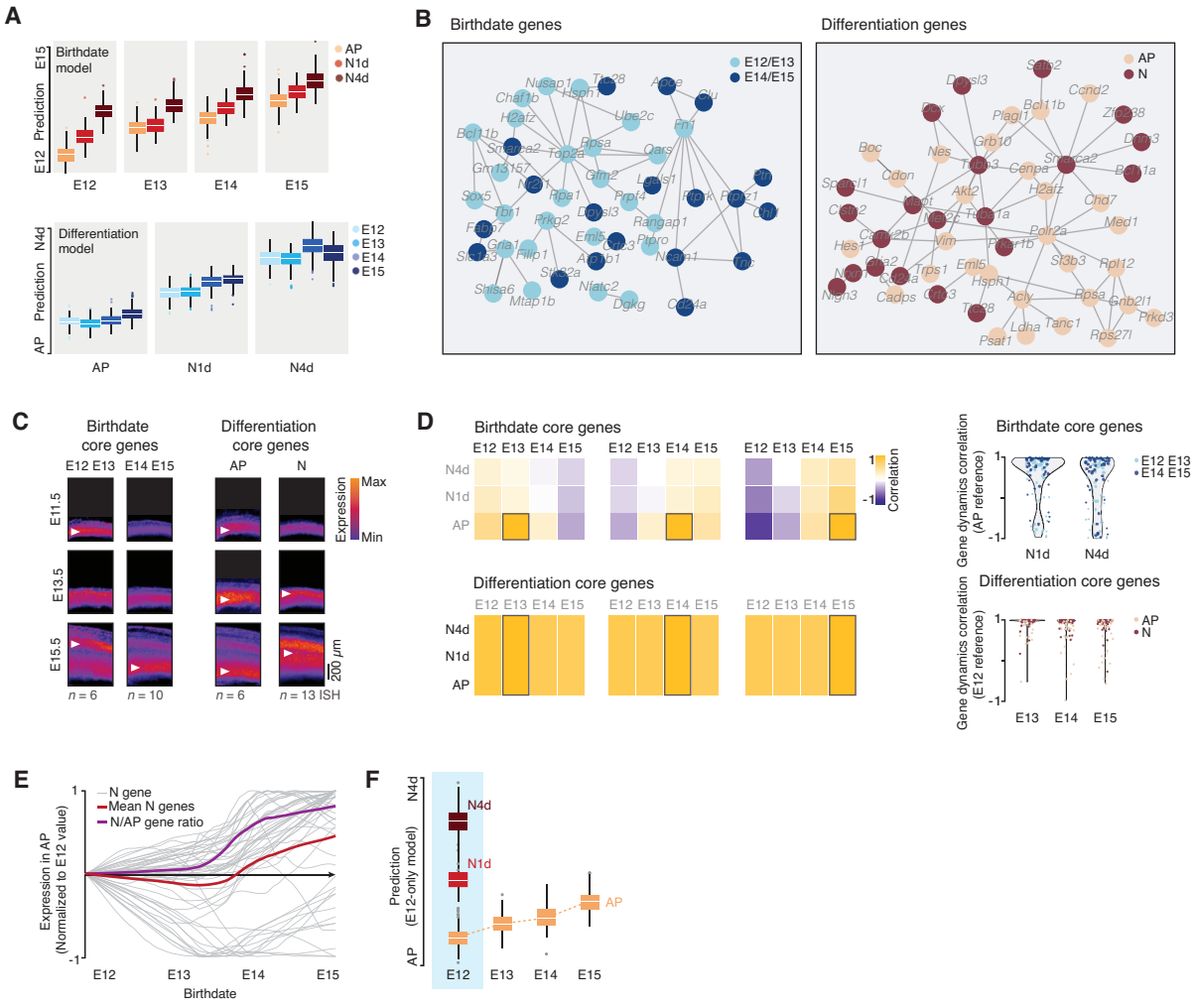

Fig. S7. 2D modelization of corticogenesis. (A) Birthdate and differentiation scores obtained from the two models for each condition. (B) Analysis of protein-protein interactions using the STRING database (http://string-db.org) suggests that gene products interact based on their temporal dynamics (left) or cellular specificity (right). Unassigned genes are not displayed. (C) Overlay of ISH from the Allen Developing Mouse Brain Atlas (www.brain-map.org) confirming the proper spatio-temporal dynamics of select core genes. Early genes: *Hes1, Hmga2, Tbr1, Fn1, Nfatc2, Sox5*. *Late genes: Nrxn1, Cttnbp2, Clu, Nr2f1, Lgals1, Bcan, Tnc, Unc5d, Slc1a3, Mfge8*. AP genes: *Cdon, Hes1, Plagl1, Nes, Hmga2, Arx*. *N genes: Trps1, Unc5d, Sox11, Nrxn, Cd24a, Mpped1, Bcl11a, Neurod6, Satb2, Dcx, Mapt, Gria2, Tubb3*. (D) Top left: Birthdate-associated core genes are temporally dynamic and daughter cells acquire embryonic stage-specific transcriptional birthmarks. Bottom left: In contrast, differentiation status-associated core genes are conserved across corticogenesis. Boxed area represents value of reference for correlation. Right: Correlations in gene expression dynamics stratified for early (E12, E13) and late (E14, E15) embryonic ages. (E) Expression of the core neuronal genes (n = 50) within APs increases with embryonic age. (F) E12-15 APs progressively become "neuronized". Differentiation model build exclusively with E12 data as a training dataset; E13-E15 APs are classified as progressively more neuron-like using this model. Abbreviations: AP: apical progenitor, N: neurons, N1d: 1-day-old neurons, N4d: 4-day-old neurons.

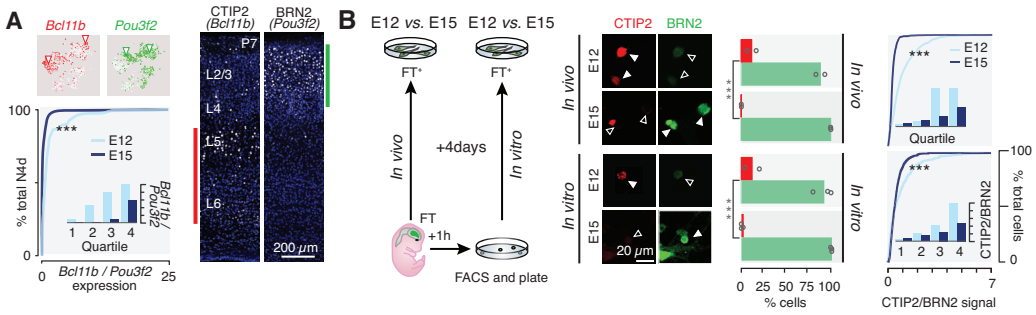

Fig. S8. Temporal patterning is still present in vitro. (A) The *Ctip2/Brn2* ratio (*i.e. Bcl11b/Pou3f2* ratio) is higher for E12-born neurons than for E15-born neurons. Top: feature plot showing expression levels, modified from S4B. Bottom: cumulative plots showing expression ratios in N4d. Right: CTIP2 and BRN2 proteins are expressed in DL and SL neurons, respectively. (B) Left: schematic of the experimen-tal setup. In both the in vivo and in vitro arm, staining is performed on dissociated cells to allow for direct comparison of CTIP2 and BRN2 expression. Center and right: neurons born from E12 and E15 APs can still be distinguished by their relative expression of CTIP2 and BRN2 in vitro, as is the case in vivo. Abbreviations: FT: FlashTag, N4d: 4-day-old neurons. *** $P < 0.001$, Fisher's exact test (for bar graph); Kolmogorov-Smirnov test (for cumulative plots).

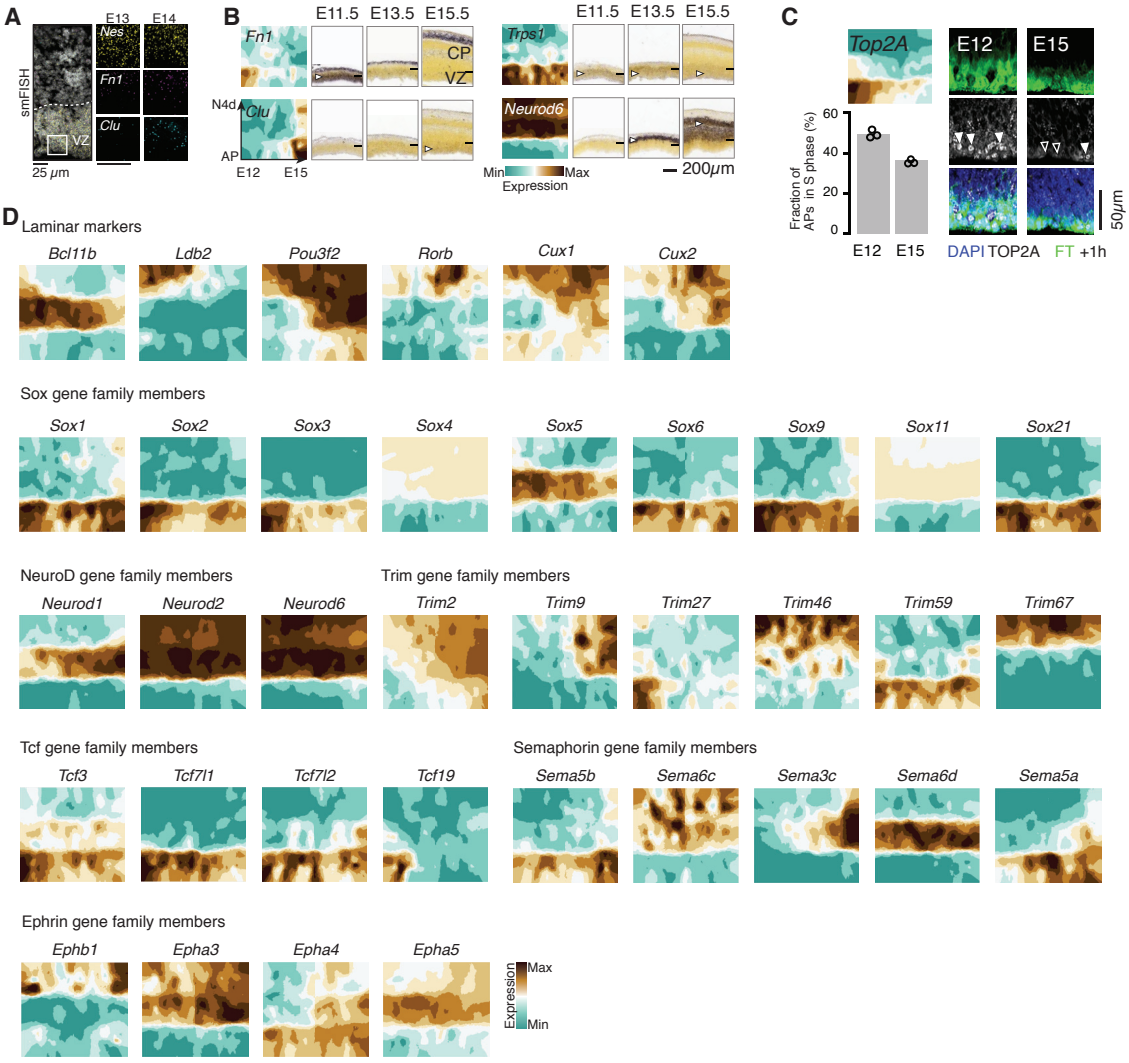

Fig. S9 Mapping of transcriptional dynamics in the developing cortex. Validation of select transcriptional patterns using (A) smFISH (see also Fig. 5B for E12 and E15 timepoints) (B) ISH from the Allen Developing Mouse Brain Atlas (www.brain-map.org) or (C) ICC. Of note, the decreased expression of *Top2A*, a S/G2-phase marker, in APs is consistent with a lengthening of the cell-cycle and a decreased proportion of S-phase APs between E12 and E15 (data from Fig. 2H analysis). (D) Transcriptional maps for select classical laminar markers and members of sample gene families. Only the genes with the most sharply delineated expression patterns are shown for Semaphorins and Ephrins. See www.genebrowser.unige.ch/telagirdon for more transcripts. Abbreviations: AP: apical progenitor, N4d: 4-day-old neurons.

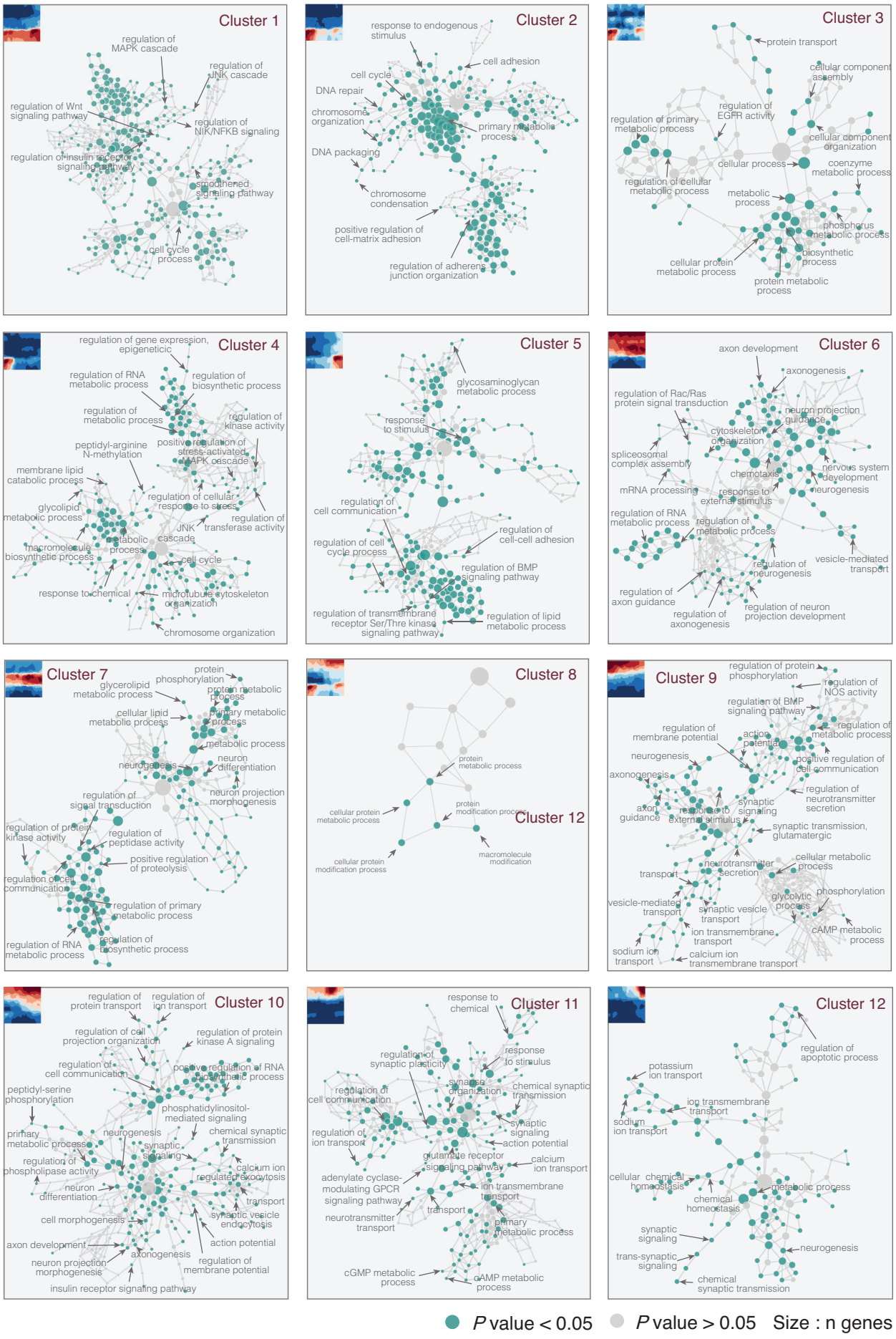

Fig. S10. Cluster-based gene ontology networks. Display of ontological hierarchies for individual clusters highlights cluster-specific biological processes.